

Tropical Pacific Climate Variability under Solar Geoengineering: Impacts on ENSO Extremes

Abdul Malik^{1,2,3}, Peer J. Nowack^{1,4,5,6}, Joanna D. Haigh^{1,4}, Long Cao⁷, Luqman Atique⁷, Yves Plancherel¹

¹Grantham Institute – Climate Change and the Environment, Imperial College London, London, United Kingdom

²Oeschger Centre for Climate Change Research, and Institute of Geography, University of Bern, Bern, Switzerland

³4700 King Abdullah University of Science and Technology, Thuwal 23955-6900, Kingdom of Saudi Arabia

⁴Department of Physics, Blackett Laboratory, Imperial College London, United Kingdom

⁵Data Science Institute, Imperial College London, United Kingdom

⁶School of Environmental Sciences, University of East Anglia, Norwich, United Kingdom

⁷School of Earth Sciences, Zhejiang University, Hangzhou, China

Correspondence to: Abdul Malik (abdul.malik@kaust.edu.sa)

Point-by-Point Listing of Response to Referee Comments

The authors thank the referees for their comments and suggestions, which have much helped us to improve our manuscript. Below, we reply point-by-point, highlighting the changes we have implemented. The response to Referee # 1 is given on pages 2-3, and for Referee # 2 on pages 4-6. The minor changes that we have made in the revised manuscript are provided on page 7.

Referee #1

Minor Revisions

1)

Add **a slight** in this sentence: “Overall there is a change in sign and reduction of MSSTG in 4×CO₂ (~111 %, 99 % cl) and only **a slight** decrease in G1 (~9 %, 99 % cl) (Fig. S3, and Table S2).” (Section 3.1.4, page 11, lines 17-19).

In the revised manuscript we have added ‘a slight’ in the text (See section 3.1.4, page 11, line 30)

2)

There are many instances where the authors state that the model can “reproduce” observed events. It would be better to replace “reproduce” (which sounds like an exact copy) with “reasonably simulate or capture”.

We have replaced the word ‘reproduce’ either with ‘capture’ or ‘simulate’ at all instances in the revised manuscript. Please see the manuscript with tracked changes.

3)

Regarding the definition of E-index and C-index, in the original definition by Takahashi et al. 2011, the first and second principal components PC1, PC2 are first normalized before calculating the E-Index, C-Index. Please ensure that this is mentioned. Takahashi et al. 2011 defined the E-Index and C-Index; Cai et al. 2018 applied these indices.

In the revised manuscript we have cited Takahashi et al. (2011) at the relevant places. We have made the following changes:

Based on Empirical Orthogonal Function Analysis (EOF) of Sea Surface Temperature (SST) in the tropical Pacific (see Takahashi et al., 2011), ENSO can be contrasted into two distinct modes of variability, i.e. eastern and central Pacific ENSO modes (Kao and Yu, 2009; Yu and Kim, 2010; Xie and Jin, 2018). (See section 1, from page 2 and line 41 to page 3, line 4)

We have cited Takahashi et al. (2011) in the following text as well:

The PCA is also useful for evaluating how well HadCM3L represents certain types of ENSO events. Eastern and central Pacific ENSO events can be described by an E-Index $(PC1-PC2)/\sqrt{2}$; Takahashi et al., 2011), which emphasises maximum warm anomalies in the eastern Pacific region (Cai et al., 2018), and a C-Index $(PC1+PC2)/\sqrt{2}$; Takahashi et al., 2011) respectively, which focuses on maximum warm anomalies in the central Pacific (Cai et al., 2018). (See section 2.4, page 8, lines 11-16)

In caption of supplementary Figure S1 we have added the following text:

The red line in m-n shows a quadratic fit between PC1 and PC2 averaged over DJF. Grey dots show monthly data whereas black dots indicate data averaged over DJF. EOF analysis is performed over the region 15° N-15° S and 140° E-80° W (Cai et al., 2018). Before analysis and calculating E- and C-index (Takahashi et al., 2011), PC1 and PC2 are normalized by their monthly standard deviations calculated over the corresponding observational and model simulation period. (See Fig. S1, Supplementary page 1, lines 11-16)

4)

P10, L24-40: On definition of Westerly Wind Burst and Easterly Wind Burst. These winds are ought to be identified using daily wind data (e.g., in Hu and Fedorov 2016). If this is not the case, please reword, e.g., “although not explicitly diagnosed, WWB and EWB are contained respectively in the positive and

negative values of this wind index.” Then please be careful with calling them WWBs and EWBs in the rest of the manuscript.

We have not omitted the use of WWBs and EWBs. Since these bursts can last for 5-40 days, thus the monthly data, which we have used in our analysis, includes monthly averages of these bursts. However, we have cited Hu and Fedorov, (2016) who calculated these bursts from daily data. In the revised manuscript we have added the following text:

Although here not explicitly diagnosed through daily data, WWBs and EWBs are contained respectively in the positive and negative values of this wind stress index (see Hu and Fedorov, 2016). As the duration of WWBs is 5 to 40 days (Gebbie et al., 2007), the monthly mean data of westerly wind stress includes a monthly average of these bursts. (See section 3.1.3, page 10, lines 37-41)

5)

P15, L10-12: “Note that Wang et al. (2020) showed that extreme convective events can still happen even if the E-index is not greater than 5 mm day⁻¹ (cf. 12 Figure 2 in Wang et al. 2020).” – E-index cannot be in the unit of mm/day.

In the revised manuscript we have rephrased the text as follows:

Note that Wang et al. (2020) showed that extreme El Niño events having E-Index > 1.5 s.d. can still happen even if the Niño3 rainfall is not greater than 5 mm day⁻¹ (cf. Figure 2 in Wang et al., 2020). (See section 3.2.2, page 15, lines 25-27)

6)

P15, L24-41: On La Nina frequency change. The fact that there are no extreme La Nina events in 4xCO₂ experiment is inconsistent with Cai et al. 2015. A remark on this is necessary to avoid confusion to description in L34-41 on G1.

We have added the following sentence in the revised manuscript:

Our findings are inconsistent to those of Cai et al. (2015b) who found nearly doubling of extreme La Nina events under increased GHG forcing. (See section 3.2.3, page 16, lines 3-5)

7)

P17, L3-23: Increased upper ocean stratification tends to enhance the Bjerknes feedback, likely through the coupling between the wind and thermocline. This is not yet diagnosed in this present analysis which instead represents the Bjerknes feedback solely on the coupling between SST and wind. The Bjerknes feedback has many components (e.g., Kim and Jin 2011), and some may increase and some may decrease under external forcing. It would be good to put a caveat like this in this paragraph.

We have added the following paragraph in Sect. 5:

Bjerknes feedback is a multi-component process (e.g., Kim and Jin, 2011a), where some components may increase and some may decrease under the influence of external forcing. For instance, increased upper ocean stratification tends to enhance the Bjerknes feedback, likely through coupling between the wind and thermocline. However, this study represents the Bjerknes feedback solely on the coupling between wind and SST, a caveat of this analysis. (See section 4.1, from page 17 and line 39 to page 18 line 4)

8)

The curve fitting in Fig. S1 (red curve) does not look a smooth parabolic.

In the revised manuscript we have replotted the red curves, hope it looks okay now. (See supplementary Fig. S1, page 2)

Referee #2

Minor Revisions

1)

P3 line3 the meaning of “until Cai et al. (2018) used SST indices basedon Principal Component Analysis (PCA).” Is not clear.

We have rephrased the text as follows:

As diagnosed from SST indices in state-of-the-art AOGCMs, there was no intermodel consensus about change in frequency of ENSO events and amplitude in a warming climate (Vega-Westhoff and Sriver, 2017; Yang et al., 2018). However recently, Cai et al. (2018), using SST indices based on Principal Component Analysis (PCA), showed an enhanced frequency of extreme El Niño events and strengthening of ENSO amplitude under increased GHG forcing. (See section 1, page 3, lines 8-13)

2)

P3 line 13-14 the meaning of eastern and central Pacific ENSO mode should be clarified in the text somewhere(see studies in Wang et al., 2019).

In the revised manuscript, we have modified the text as follows:

Based on Empirical Orthogonal Function Analysis (EOF) of Sea Surface Temperature (SST) in the tropical Pacific (see Takahashi et al., 2011), ENSO can be contrasted into two distinct modes of variability, i.e. eastern and central Pacific ENSO modes (Kao and Yu, 2009; Yu and Kim, 2010; Xie and Jin, 2018). The eastern Pacific ENSO mode (EOF1) shows maximum SST anomaly in the eastern equatorial Pacific (Niño3 region: 5° N-5° S; 150° W-90° W) whereas the central Pacific ENSO mode (EOF2) indicates maximum SST anomaly in the central Pacific (Niño4 region: 5° N-5° S; 160° E-150° W) (Kao and Yu, 2009; Cai et al., 2018). (See section 1, from page 2 and line 41 to page 3 and line 7)

3)

P3 line18 “a significant mean warming response” might be better replaced as “a significant mean state warming response”.

In the revised manuscript, we have replace “a significant mean warming response” with “a significant mean state warming response”. (See section 1, page 3, lines 27-28)

4)

P3 line 20 “CMIP 3” should be “CMIP3”.

The mentioned acronym is corrected in the revised manuscript. (See section 1, page 3, line 29)

5)

P3 line 39“argue” should be “argued”.

Corrected. (See section 1, page 4, line 6)

6)

P3 line 42 “90 %” should be “90%”.

Corrected (See section 1, page 4, line 9). We have also corrected it at all other instances in the revised manuscript. Please see manuscript with tracked changes.

7)

P6 lines 14-15 “BJ feedback is an equatorial zonal wind stress dynamic response to equatorial SST anomalies.” might be revised as “BJ feedback is a dynamical response of equatorial zonal wind stress to equatorial SST anomalies.” for clarity.

In light of the comment we have modified the text as follows:

BJ feedback is a dynamical response of equatorial zonal wind stress to equatorial SST anomalies. (See section 2.3, page 6, lines 24-25)

8)

P14 lines 5-6, the definition of extreme events is not clear, do you mean the averaged rainfall anomalies over the Niño3 region exceeding 5 mm/day? Why 5 mm/day in Cai et al. (2014) as the threshold? This should be mentioned and clarified. Is it the same reason as Wang et al. (2020)? Thus, the first paragraph in section 3.2.2 can be better organized.

No these are not rainfall anomalies, we define an extreme El Niño event for which averaged DJF Niño3 total rainfall exceeds 5 mm day^{-1} . Cai et al. (2014, 2017) used the same definition. However, we have tried to make it clear by modifying the text as follows:

We choose a threshold value of rainfall for defining extreme El Niño events based on the work of Cai et al., (2014, 2017), who chose averaged DJF Niño3 total rainfall exceeding 5 mm day^{-1} for this threshold based on observations. (See section 3.2.2, page 14, lines 20-22)

Regarding 2nd part of the comment that we should give a reason for using 5 mm/day as an extreme El Niño event threshold, the reason is already mentioned in section 2.3 (Definitions and statistical tests). We have not repeated the reason in section 3.2.2 due to redundancy. Please see the following text in Sect. 2.3, page 6, lines 8-13.

The Niño3 index is chosen for studying the characteristics of extreme El Niño events since during an extreme El Niño event, following the highest SSTs, convective activity moves towards the eastern Pacific, and the ITCZ moves over the Niño3 region resulting in rainfall higher than 5 mm day^{-1} (Cai et al., 2014). Similar to Cai et al. (2014, 2017) events with Niño3 rainfall greater than 5 mm day^{-1} are considered extreme El Niño events,.....

Further see Sect. 2.4, page 7, lines 17-20, as follows:

During extreme El Niño events, the ITCZ moves equatorward, causing significant increases in rainfall ($> 5 \text{ mm day}^{-1}$) over the eastern equatorial Pacific that skews the statistical distribution of rainfall in the Niño3 region.

9)

In section 5, the possible implications of CP ENSO frequency and amplitude changes due to atmospheric and oceanic changes under $4\times\text{CO}_2$ and G1 scenarios should be discussed. The formation of EP and CP ENSO can be distinct since BJ feedback and heat flux feedback can play a relatively different role in determining the evolution of ENSO events. As inferred from the results based on $4\times\text{CO}_2$ and G1 simulations, how might the CP ENSO be changed?

We have added the following paragraph in Sect. 5:

The changes in ENSO feedbacks and more stratified ocean temperatures under both $4\times\text{CO}_2$ and G1 can also affect the eastern and central Pacific ENSO variability differently. For instance, more stratified ocean and enhanced BJ feedback in G1 strengthens the eastern Pacific ENSO amplitude but not central Pacific ENSO amplitude (Table 1-2). Similarly, the enhanced hf and weaker BJ feedback in $4\times\text{CO}_2$ results in a more substantial reduction in central Pacific ENSO amplitude than eastern Pacific ENSO amplitude (Table 1-2). In the current model system, we expect that changes in tropical Pacific mean state and feedback process, both under $4\times\text{CO}_2$ and G1, may impact the occurrence ratio of central Pacific El Niño (La Niña) to eastern Pacific El Niño (La Niña) (e.g., Yeh et al., 2009), which requires further detailed analysis. (See section 5, page 19, lines 32-41)

Other Minor Changes that we have Made

1)

In the revised manuscript '~50-yrs' replaced with '~50-year' (See page 1, line 24)

2)

Ammedded the text '*Cai et al. (2014)*' as '*Cai et al. (2014, 2017)*'. (See page 6, line 11-12)

3)

Some typographical errors were found in Table S3, so we have modified Table S3. In the previous version this sentence '*Based on the E-index definition, we also see a statistically significant increase in the total number of El Niño events in 4×CO₂ (88%) and G1 (12 %) (Table S3).*' is thus replaced with '*Based on the E-index definition, we see a statistically significant increase in the total number of El Niño events in 4×CO₂ (107%) and no statistically significant change in G1 (Table S3).*' (See page 15, lines 23-25 or see manuscript with tracked changes)

4)

In the acknowledgement we have added the following sentence:

The authors thank the referees for their comments and suggestions, which have much helped us to improve our manuscript. (See page 21, lines 16-17)

5)

Some references were not in accordance with the journal's prescribed format; we have modified them according to the journal's instructions. Please see manuscript with tracked changes.

6)

In Fig. 4a,b the longitudinal label '80° W' was incorrectly labelled as '140° W', so we have corrected it.

7)

Some citations in the text were not in accordance with the journal's prescribed format; we have modified them according to the journal's instructions. Please see manuscript with tracked changes.

8)

In the revised manuscript '*5mm day⁻¹*' is replaced with '*5 mm day⁻¹*'. (See page 6, lines 11)

9)

In caption of Fig. S1 'ER5' is corrected as 'ERA5' and 'g-l' is corrected as 'g-i'. (See supplementary page 2, line 9 and 10)

10) For other minor changes please see the manuscript with tracked changes.

1 **Tropical Pacific Climate Variability under Solar Geoengineering: Impacts on ENSO**
2 **Extremes**

3 **Abdul Malik^{1,2,3}, Peer J. Nowack^{1,4,5,6}, Joanna D. Haigh^{1,4}, Long Cao⁷, Luqman Atique⁷,**
4 **Yves Plancherel¹**

5 ¹Grantham Institute – Climate Change and the Environment, Imperial College London,
6 London, United Kingdom

7 ²Oeschger Centre for Climate Change Research, and Institute of Geography, University of
8 Bern, Bern, Switzerland

9 ³4700 King Abdullah University of Science and Technology, Thuwal 23955-6900, Kingdom
10 of Saudi Arabia

11 ⁴Department of Physics, Blackett Laboratory, Imperial College London, United Kingdom

12 ⁵Data Science Institute, Imperial College London, United Kingdom

13 ⁶School of Environmental Sciences, University of East Anglia, Norwich, United Kingdom

14 ⁷School of Earth Sciences, Zhejiang University, Hangzhou, China

15

16 *Correspondence to:* Abdul Malik (abdul.malik@kaust.edu.sa)

17 **Abstract**

18 Many modelling studies suggest that the El Niño Southern Oscillation (ENSO), in interaction
19 with the tropical Pacific background climate, will change with rising atmospheric greenhouse
20 gas concentrations. Solar geoengineering (reducing the solar flux from outer space) has been
21 proposed as a means to counteract anthropogenic climate change. However, the effectiveness
22 of solar geoengineering concerning a variety of aspects of Earth's climate is uncertain. Robust
23 results are particularly challenging to obtain for ENSO because existing geoengineering
24 | simulations are too short (typically ~50-~~years~~^{year}) to detect statistically significant changes in
25 the highly variable tropical Pacific background climate. We here present results from a 1000-
26 year long solar geoengineering simulation, G1, carried out with the coupled atmosphere-
27 ocean general circulation model HadCM3L. In agreement with previous studies, reducing the
28 | solar irradiance (4-%) to offset global mean surface warming in the model more than
29 compensates the warming in the tropical Pacific that develops in the 4×CO₂ scenario. We see
30 | an overcooling of 0.3°C and a 0.23-mm day⁻¹ (5-%) reduction in mean rainfall over tropical
31 Pacific relative to preindustrial conditions in the G1 simulation, owing to the different
32 latitudinal distributions of the shortwave (solar) and longwave (CO₂) forcings. The location
33 of the Intertropical Convergence Zone (ITCZ) in the tropical Pacific, which moved 7.5°
34 southwards under 4×CO₂, is restored to its preindustrial position. However, other aspects of
35 the tropical Pacific mean climate are not reset as effectively. Relative to preindustrial
36 conditions, in G1 the time-averaged zonal wind stress, zonal sea surface temperature (SST)
37 gradient, and meridional SST gradient are each statistically significantly reduced by around
38 | 10-%, and the Pacific Walker Circulation (PWC) is consistently weakened resulting in
39 conditions conducive to increased frequency of El Niño events. The overall amplitude of
40 | ENSO strengthens by 9-10% in G1, but there is a 65 % reduction in the asymmetry between
41 cold and warm events: cold events intensify more than warm events. Notably, the frequency
42 | of extreme El Niño and La Niña events increases by ca. 60-0% and 30-0%, respectively, while
43 the total number of El Niño events increases by around 10-0%. All of these changes are

1 | statistically significant either at 95 or 99-% confidence level. Somewhat paradoxically, while
2 | the number of total and extreme events increases, the extreme El Niño events become weaker
3 | relative to the preindustrial state while the extreme La Niña events become even stronger.
4 | That is, such extreme El Niño events in G1 become less intense than under preindustrial
5 | conditions, but also more frequent. In contrast, extreme La Niña events become stronger in
6 | G1, which is in agreement with the general overcooling of the tropical Pacific in G1 relative
7 | to preindustrial conditions.

8 | **1 Introduction and Background**

9 | Since the industrial revolution, anthropogenic emissions of Greenhouse Gases (GHGs) have
10 | led to globally increasing surface temperatures (Stocker, 2013). Higher temperatures, in turn,
11 | and more generally a rapidly changing climate, can have adverse effects on humans, plants,
12 | and animals through changes in various ecosystems, rising sea levels, melting glaciers, and
13 | could significantly impact the frequency and intensity of extreme weather events (Moore et
14 | al., 2015). Various strategies, principally a reduction of GHG emissions and enhancements of
15 | carbon dioxide sinks (Pachauri et al., 2014), have been proposed to mitigate anthropogenic
16 | climate change. Another group of strategies involves the intentional modification of Earth's
17 | radiation balance on a global scale, known as solar geoengineering (Crutzen, 2006; Wigley,
18 | 2006; Curry et al., 2014). For any serious consideration of such geoengineering strategies, it
19 | is essential to understand their potential perils as well as benefits. One route to study the
20 | potential impacts of geoengineering on various components of Earth's climate system (e.g.,
21 | atmosphere, ocean, cryosphere, etc.) is through employing state-of-the-art coupled
22 | atmosphere-ocean general circulation models (AOGCMs).

23 | In this context, Kravitz et al. (2011) proposed the Geoengineering Model Intercomparison
24 | Project (GeoMIP), which initially consisted of a set of four experiments (viz. G1, G2, G3,
25 | and G4). These experiments are designed to investigate the effects of geoengineering on the
26 | regional and global climate when it is implemented to offset the annual mean global radiative
27 | forcing at the top of the Earth's atmosphere introduced by GHGs. These experiments are
28 | collectively called Solar Radiation Management (SRM) or solar geoengineering (Kravitz et
29 | al., 2013a). In the G1 experiment, atmospheric CO₂ is instantaneously quadrupled, but the
30 | global GHG-induced longwave radiative effects are offset by a simultaneous reduction in the
31 | shortwave Total Solar Irradiance, TSI, (Kravitz et al., 2011). In terms of radiative forcing, the
32 | quadrupling of CO₂ is similar to the year 2100 in the RCP8.5 emission scenario
33 | (Representative Concentration Pathway with a radiative forcing of 8.5 W m⁻² by the year
34 | 2100; Schmidt et al., 2012). In this paper, we focus on the G1 experiment to investigate how
35 | effectively solar geoengineering could mitigate the effects of substantial changes in
36 | atmospheric CO₂ on the tropical Pacific climate.

37 | The El Niño Southern Oscillation (ENSO) is an important coupled ocean-atmosphere mode
38 | of interannual variability in the tropical Pacific (Park et al., 2009; Vecchi and Wittenberg
39 | 2010), which affects both regional and global climate (see Ropelewski and Halpert, 1987;
40 | Bove et al., 1998; Malik et al., 2017). ENSO oscillates between a warm, El Niño, and a cold,
41 | La Niña, phase every 2-7-year (Santoso et al., 2017). ~~As diagnosed from Sea Surface~~

1 ~~Temperature (SST)~~Based on Empirical Orthogonal Function Analysis (EOF) of Sea Surface
2 ~~Temperature (SST) in the tropical Pacific (see Takahashi et al., 2011), ENSO can be~~
3 ~~contrasted into two distinct modes of variability, i.e. eastern and central Pacific ENSO modes~~
4 ~~(Kao and Yu, 2009; Yu and Kim, 2010; Xie and Jin, 2018). The eastern Pacific ENSO mode~~
5 ~~(EOF1) shows maximum SST anomaly in the eastern equatorial Pacific (Niño3 region: 5° N-~~
6 ~~5° S; 150° W-90° W) whereas the central Pacific ENSO mode (EOF2) indicates maximum~~
7 ~~SST anomaly in the central Pacific (Niño4 region: 5° N-5° S; 160° E-150° W) (Kao and Yu,~~
8 ~~2009; Cai et al., 2018).~~

9 ~~As diagnosed from SST~~ indices in state-of-the-art AOGCMs, there was no intermodel
10 consensus about change in frequency of ENSO events and amplitude in a warming climate
11 (Vega-Westhoff and Sriver, 2017; Yang et al., 2018) ~~until~~. ~~However recently,~~ Cai et al.
12 (2018) ~~used~~, ~~using~~ SST indices based on Principal Component Analysis (PCA) ~~), showed an~~
13 ~~enhanced frequency of extreme El Niño events and strengthening of ENSO amplitude under~~
14 ~~increased GHG forcing~~. However, before that, Cai et al. (2014 and 2015b) also showed
15 evidence of a doubling of El Niño and La Niña events in the Coupled Model Intercomparison
16 Project (CMIP) phases 3 (A2 scenario) and 5 (RCP8.5) by investigating a performance-based
17 subset of models using rainfall-based ENSO indices instead of SST-based indices. Similarly,
18 Wang et al. (2017) also reported a doubling of extreme El Niño events, relative to the
19 preindustrial level, in the RCP2.6 transient scenario a century after stabilization of global
20 mean temperature. Chen et al. (2017), ~~analyzing~~~~analysing~~ 20 CMIP5 models (RCP8.5), found
21 both strengthening (in 6 models) and weakening (in 8 models) of ENSO amplitude. However,
22 Cai et al. (2018) later found robust evidence of a consistent increase in El Niño amplitude in
23 the subset of CMIP5 climate models, which were capable of ~~reproducing~~~~simulating~~ both
24 eastern and central Pacific ENSO modes. In summary, changes in ENSO characteristics such
25 as amplitude and ENSO extremes are projected in a warming climate (e.g., Cai et al., 2014,
26 2015b, 2018; Kim et al., 2014; Wang et al., 2018).

27 Increasing GHGs have distinct effects on the tropical Pacific mean climate. In CMIP3 and
28 CMIP5 simulations, the equatorial tropical Pacific consistently shows a significant mean ~~state~~
29 warming response to increased GHG forcing (van Oldenborgh et al., 2005; Collins et al.,
30 2010; Vecchi and Wittenberg 2010; Huang and Ying 2015; Luo et al., 2015). ~~CMIP-3~~~~CMIP3~~
31 and CMIP5 models generally show more warming on than off-equatorial tropical Pacific (Liu
32 et al., 2005; Collins et al., 2010; Cai et al., 2015a). Consistent with these warming patterns,
33 studies typically found a weakening of zonal SST gradient (ZSSTG), Pacific Walker
34 Circulation (PWC), zonal wind stress, and a shoaling of the equatorial tropical Pacific
35 thermocline (see van Oldenborgh et al., 2005; Latif et al., 2009; Park et al., 2009; Yeh et al.,
36 2009; Collins et al., 2010; Kim et al., 2014; Cai et al., 2015a; Zhou et al., 2015; Coats and
37 Karnauskas 2017; Vega-Westhoff and Sriver 2017). Changes in the mean state of the tropical
38 Pacific can bring about variations in ENSO properties such as amplitude, frequency, and
39 spatial pattern (Collins et al., 2010; Vecchi and Wittenberg, 2010; Cai et al., 2015a).

40 We note that a previous study by Guo et al. (2018) found no statistically significant change in
41 the intensity of Walker Circulation in GeoMIP models when comparing preindustrial
42 simulations to the G1 experiment. Similarly, Gabriel and Robock (2015) found no

1 statistically significant change in frequency and amplitude of ENSO events under both global
2 warming and geoengineering scenarios in 6 GeoMIP models that captured ENSO variability
3 best. However, these authors themselves highlighted the length of their simulations (~50
4 years) as a key constraint for their studies. They suggested that long term simulations (>50
5 years) would be required to detect possible ENSO changes. Guo et al. (2018) concluded that
6 60 or more years of model simulations are required to detect changes in the PWC, while
7 Vecchi et al. (2006) and Vecchi and Soden (2007) ~~argue~~argued that 130-yr are necessary to
8 identify any robust change in the PWC (Gabriel and Robock, 2015). Similarly, Stevenson et
9 al. (2010) estimated that 250 years are needed to detect changes in ENSO variability with a
10 statistical significance of 90-%. Here we aim to address this gap in the literature and establish
11 a baseline for future studies through the analysis of long-term (1000 year) simulations of a
12 single climate model.

13 Here, we employ three 1000-year long climate model simulations (preindustrial forcing,
14 abrupt-4xCO₂ forcing, and G1) to estimate the efficacy of solar geoengineering in resetting
15 the tropical Pacific circulation. Specifically, we investigate: (1) if solar geoengineering can
16 mitigate the changes in mean tropical Pacific climate found in previous GHG warming
17 studies, and even bring it back to the preindustrial conditions; (2) if ENSO frequency and
18 amplitude are different under G1 conditions than under preindustrial simulations; and (3) if
19 the G1 experiment reduces the increase in the frequency of extreme ENSO events, as shown
20 by Cai et al. (2014, 2015b and 2018), under increased GHG forcing, relative to the
21 preindustrial state. For this purpose, we are primarily interested in the more subtle differences
22 in climate between G1 and preindustrial conditions, but also consider the profound changes
23 under 4xCO₂ where, by design, the global mean surface temperature is much higher, and thus
24 many other climate aspects vastly differ from the other two scenarios.

25 Section 2 describes the climate model HadCM3L, the data and the statistical methods used to
26 detect changes in tropical Pacific and ENSO variability. The same section also evaluates the
27 capability of HadCM3L to model ENSO. Section 3 evaluates the response of a list of metrics
28 used to understand how the mean state and ENSO variability are affected in different
29 experiments (preindustrial, 4xCO₂, G1). Section 4 elaborates on the mechanism of ENSO
30 variability under GHG forcing and solar geoengineering for the given model system. Finally,
31 Section 5 presents the discussion and conclusions.

32 **2 Data and methods**

33 **2.1 Climate model**

34 HadCM3L (Cox et al., 2000) has a horizontal resolution of 2.5° latitude × 3.75° longitude
35 (~T42) with 19 (L19) atmospheric and 20 (L20) ocean levels. HadCM3L stems from the
36 family of HadCM3 climate models; the only difference is lower ocean resolution (HadCM3:
37 1.25° × 1.25°; Valdes et al., 2017). In HadCM3L, land surface processes are simulated by the
38 MOSES-2 module (Essery and Clark, 2003; Cao et al., 2016). HadCM3L does not include an
39 interactive atmospheric chemistry scheme and thus does not consider effects of ozone
40 changes on ENSO amplitude and surface warming under 4xCO₂ (e.g., Nowack et al., 2015;

1 2017, 2018) or G1 (e.g., Nowack et al., 2016). Instead, we use preindustrial background
2 ozone climatology, prescribed on pressure levels. In section 2.4, we evaluate the ability of
3 HadCM3L to model ENSO. We acknowledge that some of our results will necessarily be
4 model-dependent, and underline the need for similar studies with other climate models. Still,
5 by using much longer simulations than used previously, our results provide statistical
6 robustness for the given model system.

7 2.2 Simulations and observational data

8 Here, we use HadCM3L simulations carried out by Cao et al. (2016). To achieve a quasi-
9 equilibrium preindustrial climate state, the model was spun up for 3000 years with constant
10 CO₂ concentrations (280 ppmv; parts per million by volume) and TSI (1365 W m⁻²). Then,
11 three 1000-year long experiments were carried out, starting from this preindustrial climate
12 state. These experiments are: (1) the preindustrial control (piControl) experiment with
13 constant values of CO₂ (280 ppmv) and TSI (~~1365 W~~ 1365 W m⁻²); (2) a quadrupled CO₂
14 (4×CO₂) experiment in which CO₂ is suddenly increased to 1120 ppmv; and (3) sunshade
15 geoengineering (G1) experiment where the radiative effects of the instantaneously
16 quadrupled CO₂ are offset by simultaneously reducing TSI (by 4-%). All experiments follow
17 the GeoMIP protocol (see Kravitz et al., 2011); the only difference being that simulations
18 were run for 1000 years (see Cao et al., 2016) instead of 50 years as in GeoMIP.

19 The monthly SST dataset from HadISST (1° latitude × 1° longitude; Rayner et al., 2003) and
20 the rainfall data from the Global Precipitation Climatology Project (GPCP; Adler et al., 2003)
21 version 2.3 (2.5° latitude × 2.5° longitude) over the period 1979-2017 are used to provide
22 observational constraints and to identify the rainfall threshold to be used for defining extreme
23 El Niño events. Further, we use ERA5 reanalysis data (Copernicus Climate Change Service
24 (C3S), 2017) covering years 1979-2019 to evaluate the capability of HadCM3L to simulate
25 ENSO variability. ERA5 has a horizontal resolution of 0.25° latitude × 0.25° longitude.
26 Specifically, we use monthly mean surface latent heat flux (lh), sensible heat flux (sh), net
27 shortwave radiation flux (sw), net longwave radiation flux (lw), ocean temperature, and zonal
28 and meridional components of wind stress.

29 2.3 Definitions and statistical tests

30 We ~~analyze~~ analyze changes in the tropical Pacific (25° N-25° S; 90° E-60° W) mean climate.
31 We present climatologies for SSTs, rainfall, Intertropical Convergence Zone (ITCZ), vertical
32 velocity averaged between 500 and 100 hPa (Omega500-100), PWC, zonal wind stress, zonal
33 and meridional SST gradients (ZSSTG and MSSTG, respectively), and thermocline depth.
34 We calculate mean climatological differences for all these variables simulated under 4×CO₂
35 and G1 relative to piControl and assess their statistical significance using non-parametric
36 Wilcoxon signed-rank and Wilcoxon rank-sum tests (Hollander and Wolfe, 1999; Gibbons
37 and Chakraborti, 2011). All analyses are performed on re-gridded (2° longitude × 2.5°
38 latitude) HadCM3L output for model years 11 to 1000 unless otherwise stated. The first
39 ~~10~~ten years are skipped to remove the initially significant atmospheric transient effects
40 stemming from instantaneously increasing CO₂ (see Kravitz et al., 2013b; Hong et al., 2017).

1 Since ENSO events peak in boreal winter (December-January-February; DJF; Cai et al.,
2 2014; Gabriel and Robock 2015; Santoso et al., 2017), the entire analysis is performed for
3 DJF, unless otherwise stated. Accordingly, we also ~~analyze~~analyse mean state changes in the
4 tropical Pacific during boreal winter.

5 Both rainfall and SST-based ENSO indices are used in the present study. Niño3 (5° N-5° S;
6 150° W-90° W) and Niño4 (5° N-5° S; 160° E-150° W) indices are defined by averaging SST
7 over corresponding ENSO regions. ~~Normalized~~Normalised ENSO anomalies (i.e., the ENSO
8 indices) are calculated relative to piControl mean and standard deviation (s.d.) and are
9 quadratically detrended before analysis. The Niño3 index is chosen for studying the
10 characteristics of extreme El Niño events since during an extreme El Niño event, following
11 the highest SSTs, convective activity moves towards the eastern Pacific, and the ITCZ moves
12 over the Niño3 region resulting in rainfall higher than ~~5mm~~5 mm day⁻¹ (Cai et al., 2014).
13 Similar to Cai et al. (2014, 2017), events with Niño3 rainfall greater than 5 mm day⁻¹ are
14 considered extreme El Niño events, whereas events with Niño3 SST index greater than 0.5
15 s.d. and Niño3 rainfall less than 5 mm day⁻¹ are defined as moderate events unless otherwise
16 stated. The Niño4 index is chosen for studying the characteristics of extreme La Niña events
17 since maximum cold temperatures occur in this region (Cai et al., 2015a, 2015b). La Niña
18 extreme (Niño4 < -1.75 s.d.), moderate (-1 > Niño4 > -1.75), and weak (-0.5 > Niño4 > -1)
19 events are defined following Cai et al. (2015b). These definitions classify the 1988 and 1998
20 La Niñas in observations as extreme events (see Cai et al., 2015b), and HadCM3L can
21 ~~reproduce~~capture such extreme anomalies (see Sect. 3.2), which allows us to study changes in
22 their number and magnitude.

23 To understand the mechanisms responsible for changes in ENSO variability, we have
24 calculated ENSO feedbacks (e.g., Bjerkness (BJ) and heat flux (hf) feedbacks) and ocean
25 stratification. BJ feedback is ~~ana~~ dynamical response of equatorial zonal wind stress ~~dynamic~~
26 ~~response~~ to equatorial SST anomalies. It is positive feedback that maintains the ZSSTG
27 (Lloyd et al., 2011). Here, we calculate the BJ feedback by point-wise linear regression
28 (Bellenger et al., 2014) of the zonal wind stress anomalies over the entire equatorial Pacific
29 (5° N-5° S; 120° E-80° W; Kim ~~et al., 2011~~and Jin 2011a; Ferret ~~et al., and Collins~~ 2019) onto
30 the eastern equatorial Pacific (5° N-5° S; 180° W-80° W; Kim ~~et al., 2011~~and Jin 2011a;
31 Ferret ~~et al., and Collins~~ 2019) SST anomalies. We then define the BJ feedback as the mean
32 regression coefficient (Bellenger et al., 2014) over the eastern equatorial Pacific region. The
33 hf feedback is a regression coefficient calculated by point-wise linearly regressing the net
34 surface heat flux (sum of sw, lw, lh, and sh) anomalies into the ocean onto the SST anomalies
35 over the eastern equatorial Pacific (5° N-5° S; 180° W-80° W; Kim and Jin 2011a). This
36 regression coefficient is also termed as a thermal damping coefficient (Kim and Jin, 2011a).
37 It is ~~a~~ negative feedback in which an initial positive SST anomaly causes a reduced surface
38 net heat flux into the ocean, thus lessening the initial SST anomaly (Lloyd et al., 2011).
39 Ocean stratification is defined as the difference in the volumetric average of ocean
40 temperatures over the upper 67 m, and the temperature of a single ocean layer at 95 m, both
41 spatially averaged over the region, 5° N-5° S; 150° E-140° W, where strong zonal wind stress
42 anomalies also occur (see Fig. 4a and Fig. S1; Cai et al., 2018).

1 Following Cai et al. (2014), the statistical significance of the change in the frequency of
2 ENSO events is tested using a bootstrap method with 10,000 ~~realizations~~realisations for the
3 piControl data. We then find the s.d. of events over these 10,000 ~~realizations~~realisations. If
4 the difference of events of piControl with 4xCO₂ and G1 is larger than 2 s.d., the change in
5 frequency is considered statistically significant. The same method is used for testing the
6 statistical significance of a change in ENSO amplitude, ZSSTG, MSSTG, ENSO amplitude
7 asymmetry, ENSO feedbacks, and ocean stratification. All changes in 4xCO₂ and G1 are
8 described relative to piControl.

9 2.4 ENSO representation in HadCM3L

10 Before employing HadCM3L for studying ENSO variability under 4xCO₂, and G1, we
11 evaluate its piControl simulation against present-day observational data. There is a non-linear
12 relationship between tropical Pacific SST and rainfall (Ham, 2017), which can be diagnosed
13 by Niño3 region rainfall skewness (Cai et al., 2014). Skewness is a measure of asymmetry
14 around the mean of the distribution (see eq. S1). Positive skewness means that in given data
15 distribution, the tail of the distribution is spread out towards high positive values, and vice
16 versa (Ghandi et al., 2016). The skewness criterion is used to exclude climate models
17 simulating overly wet or dry conditions over the Niño3 region (Cai et al., 2017). During
18 extreme El Niño events, the ITCZ moves equatorward, causing significant increases in
19 rainfall (> 5 mm day⁻¹) over the eastern equatorial Pacific that skews the statistical
20 distribution of rainfall in the Niño3 region. Thus, for studying extreme ENSO events, the
21 model should be capable of simulating Niño3 rainfall above 5 mm day⁻¹ and Niño3 rainfall
22 skewness of greater than 1 over the entire simulated period (see our Sect. 3.2.2, and Cai et al.,
23 2014 and 2015b). With a Niño3 rainfall skewness of 2.06 for piControl, HadCM3L fulfils
24 this criterion.

25 In addition, we evaluate the ENSO modelled by HadCM3L following a principal component
26 (PC) approach suggested by Cai et al. (2018). Considering distinct eastern and central Pacific
27 ENSO regimes based on ~~Empirical Orthogonal Function (EOF)~~ analysis, they found that
28 climate models capable of ~~reproducing~~simulating present-day ENSO diversity show a robust
29 increase in eastern Pacific ENSO amplitude in a greenhouse warming scenario. Specifically,
30 the approach assumes that any ENSO event can be represented by performing EOF analysis
31 on monthly SST anomalies and combining the first two principal patterns (Cai et al., 2018).
32 The first two PCs time series, PC1 and PC2, show a non-linear relationship in observational
33 datasets (Fig. S1m). Climate models that do not show such a non-linear relationship cannot
34 satisfactorily ~~reproduce~~simulate ENSO diversity, and hence are not sufficiently skilful for
35 studying ENSO properties (Cai et al., 2018). Here, we perform EOF analysis on quadratically
36 detrended monthly SST and wind stress anomalies of ERA5 and piControl over a consistent
37 period of 41-year. We evaluate HadCM3L's ability to simulate two distinct ENSO regimes
38 and the non-linear relationship between the first two PCs, i.e., $PC2(t) = \alpha[PC1(t)]^2 +$
39 $\beta[PC1(t)] + \gamma$ (Fig. S1). From ERA5, $\alpha = -0.36$ (statistically significant at 99-% confidence
40 level, hereafter “cl”) whereas in piControl $\alpha = -0.31$ (99-% cl), which is same as the mean $\alpha =$
41 -0.31 value calculated by Cai et al. (2018) averaged over five reanalysis datasets. The 1st and
42 2nd EOF patterns of monthly SST and wind stress anomalies of piControl (Fig. S1 b, e) are

1 comparable with that of ERA5 (Fig. S1 a, d). EOF1 of piControl shows slightly stronger
2 warm anomalies in the eastern equatorial Pacific, whereas negative anomalies over the
3 western Pacific are slightly weaker compared to ERA5. In EOF1, the stronger wind stress
4 anomalies occur to the west of the Niño3 region, which is a characteristic feature during the
5 eastern Pacific El Niño events (see Kim and Jin, 2011a). Compared to ERA5, the spatial
6 pattern of warm eastern Pacific anomalies is slightly stretched westwards, and wind stress
7 anomalies are relatively stronger over the equator and South Pacific Convergence Zone
8 (SPCZ). The 2nd EOF, in both ERA5 and piControl, shows warm SST anomalies over the
9 equatorial central Pacific Niño4 region. The variance distributions for ERA5 and HadCM3L
10 match well for EOF1 (ERA5: 82-%, piControl: 90-%) whereas a large difference exist for
11 EOF2 (ERA5: 18-%, piControl: 10-%).

12 The PCA is also useful for evaluating how well HadCM3L represents certain types of ENSO
13 events. Eastern and central Pacific ENSO events can be described by an E-Index $(PC1-$
14 $PC2)/\sqrt{2}$; Takahashi et al., 2011), which ~~emphasizes~~ ~~emphasises~~ maximum warm anomalies in
15 the eastern Pacific region; (Cai et al., 2018), and a C-Index $(PC1+PC2)/\sqrt{2}$; Takahashi et al.,
16 2011) respectively, which focuses on maximum warm anomalies in the central Pacific (Cai et
17 al., 2018). Here, we show the eastern Pacific (EP) Pattern (Fig. S1 g, h) and central Pacific
18 (CP) pattern (Fig. S1 j, k) by linear regression of mean DJF E- and C-Index, respectively,
19 onto mean DJF SST and wind stress anomalies. We find that model's EP and CP patterns
20 agree reasonably well with that of ERA5. HadCM3L underestimates the E-index skewness
21 (1.16) whereas overestimates the C-Index skewness (-0.89) compared to ERA5 (2.08 and -
22 0.58, respectively) averaged over DJF. HadCM3L's performance averaged over the entire
23 simulated period of piControl is also consistent with ERA5 (Fig. S1; α : -0.32, EOF1: 64-%,
24 EOF2, 8%, E-index skewness: 1.30, C-index skewness: -0.42). In general, in HadCM3L, the
25 contrast between the E- and C-index skewness over the entire simulated period is sufficient
26 enough to differentiate relatively strong warm (cold) events in the eastern (central) equatorial
27 Pacific compared to the central (eastern) equatorial Pacific. Finally, we also evaluated the hf
28 and BJ feedbacks which, for piControl, are very similar to those of ERA5 (Table S5-6).

29 We conclude that HadCM3L has a reasonable skill for studying long-term ENSO variability
30 and its response to solar geoengineering. However, we also highlight the need for and hope to
31 motivate future modelling studies that will help identify model dependencies in the ENSO
32 response.

33 3 Results

34 3.1 Changes in the tropical Pacific mean state

35 In this section, we ~~analyze~~ ~~analyse~~ several significant changes in the tropical Pacific mean
36 state under 4xCO₂ and G1. In particular, we look into meridional and zonal SST changes,
37 corresponding surface wind responses, and coupled variations in the thermocline depth. Our
38 analysis reveals that this leads to significant changes in the precipitation climatology among
39 the simulations. Finally, we find consistent effects on the PWC. All these results are

1 important not just as general climatic features but also because they are mechanistically
2 linked to changes in ENSO extremes discussed in detail in Sect. 3.2.

3 3.1.1 Sea surface temperature

4 Tropical Pacific SSTs are spatially asymmetric along the equator. The western equatorial
5 Pacific (warm pool) is warmer on average than the eastern equatorial Pacific (cold tongue)
6 (Vecchi and Wittenberg, 2010). The piControl simulation (Fig. 1a) ~~reproduces reasonably~~
7 simulates the SST asymmetry between the western and eastern equatorial Pacific well (cf. Fig
8 1a in Vecchi and Wittenberg, 2010). Under 4×CO₂, the SST zonal asymmetry is significantly
9 reduced (Fig. 1b), and the entire equatorial tropical Pacific shows a warming state (e.g.,
10 Meehl and Washington, 1996; Boer et al., 2004). The solar dimming in G1 largely offsets the
11 warming seen under 4×CO₂ and brings the tropical Pacific mean SSTs close to the
12 preindustrial state (Fig. 1c). The SPCZ, where the highest SSTs of the warm pool occur (Cai
13 et al., 2015a; blue line in Fig. 1a), moves towards the equator under 4×CO₂ (blue line, Fig.
14 1b), but returns to approximately its preindustrial position in G1 (Fig. 1c).

15 The tropical Pacific is ~~3.90-°C90°C~~ warmer in 4×CO₂ but 0.30 °C colder in G1, with both
16 differences being significant at the 99-% cl (see Fig. 1d-e, Table S1). The Pacific cold tongue
17 warms more rapidly than the Pacific Warm Pool under 4×CO₂. In contrast, in G1, a stronger
18 cooling occurs in the Pacific Warm Pool and the SPCZ than in the cold tongue region. The
19 Pacific Warm Pool is ~0.4-0.6 °C colder in G1, whereas the east Pacific cools less (~-0.2 °C
20 in the Niño3 region), indicating a change in SST asymmetry under G1.

21 Our SST results under 4×CO₂ qualitatively agree with previous studies (Liu et al., 2005; van
22 Oldenborgh et al., 2005; Collins et al., 2010; Vecchi and Wittenberg ~~et al.~~, 2010; Cai et al.,
23 2015a; Huang and Ying ~~et al.~~, 2015; Luo et al., 2015; Kohyama et al., 2017; Nowack et al.,
24 2017). Overcooling of the tropics (and as such, the tropical Pacific) is a robust signal in G1
25 simulations, even short ones, simply due to the different meridional distribution of shortwave
26 and longwave forcing (Govindasamy and Caldeira, 2000; Lunt et al., 2008; Kravitz et al.,
27 2013b; Curry et al., 2014; Nowack et al., 2016). The results presented here based on a long
28 simulation not only corroborate previously published findings but also statistically
29 demonstrate that under G1, the Warm Pool and SPCZ cool faster than the cold tongue.

30 3.1.2 Precipitation

31 In the tropical Pacific, there are three dominant bands of rainfall activity: one in the western
32 Pacific Warm Pool, one in the SPCZ, and the last one along the ITCZ situated at around 8° N
33 and 150° W-90° W. Further, the eastern equatorial Pacific is relatively dry compared with
34 these three rainy bands (cf. Fig. 2a Sun et al. 2020). Under piControl, HadCM3L simulates
35 these spatial rainfall patterns well, with maxima of ~6-8, ~12-14, and ~8-10 mm day⁻¹ over
36 the Pacific Warm Pool, the SPCZ, and the ITCZ, respectively (Fig. 2a). Under 4×CO₂, the
37 spatial rainfall pattern changes significantly. The ITCZ moves equatorward, and the SPCZ
38 becomes zonally oriented (blue line, Fig. 2b). The rainfall asymmetry between the western
39 and eastern equatorial Pacific decreases under 4×CO₂. Precipitation migrates from the west
40 Pacific to the Niño3 region, with maximum rainfall at ~145° W. The reduced zonal

1 asymmetry in the rainfall between western and eastern Pacific is effectively restored to the
2 preindustrial state in G1 (Fig. 2c).

3 | A statistically significant (99-% cl) overall precipitation increase of 0.21 mm day^{-1} (+5-%) is
4 seen over the tropical Pacific under $4\times\text{CO}_2$ (Fig. 2d). In contrast, the mean rainfall in G1
5 | decreases by 0.23 mm day^{-1} (-5-%; Fig. 2e), consistent with the simulated reduction in
6 temperature ($-0.30 \text{ }^\circ\text{C}$) over the tropical Pacific. However, there is a strong regional structure:
7 under $4\times\text{CO}_2$, rainfall decreases to a maximum of $\sim 3 \text{ mm day}^{-1}$ over parts of the Pacific
8 Warm Pool and off-equatorial regions, whereas a significant increase of $\sim 15\text{-}18 \text{ mm day}^{-1}$
9 develops over the Niño3 region. An overall increase in mean rainfall under the GHG
10 warming scenario has also been reported in many previous studies (e.g., Watanabe et al.,
11 | 2012; [Power et al., 2013](#); Chung et al., 2014; [Power et al., 2013](#); Nowack et al., 2016). Under
12 G1, rainfall decreases over the Pacific Warm Pool, SPCZ, and ITCZ regions. In contrast,
13 rainfall increases significantly over most parts of central and eastern equatorial Pacific, with a
14 maximum ($\sim 1.5\text{-}2 \text{ mm day}^{-1}$) centred at $\sim 150^\circ \text{ W}$ (Fig. 2e). Kravitz et al. (2013b) reported a
15 decrease of 0.2 mm day^{-1} over the tropical regions. Under G1, the magnitude of the lapse rate
16 decreases, resulting in increased atmospheric stability and hence suppressed convection,
17 which leads to an overall reduction of rainfall over the tropics (Bala et al., 2008; Kravitz et
18 al., 2013b).

19 The position of the ITCZ over the tropical Pacific ($25^\circ \text{ N}\text{-}25^\circ \text{ S}$; $90^\circ \text{ E}\text{-}60^\circ \text{ W}$) is calculated by
20 finding the latitude of maximum rainfall (blue lines, Fig. 2a-e). The median position of this
21 maximum ITCZ (from $154^\circ \text{ W}\text{-}82^\circ \text{ W}$) is 7.5° N , 0° , and 7.5° N under piControl, $4\times\text{CO}_2$, and
22 G1, respectively. Thus, under $4\times\text{CO}_2$, the ITCZ mean position shifts over the equator and is
23 positioned within the Niño3 region. G1 restores the ITCZ and SPCZ to their preindustrial
24 orientations. Still, differences in the magnitude of rainfall persist over these regions, as well
25 as over the Pacific Warm Pool (Fig. 2a, c, e). That is, while the relative additional rainfall
26 asymmetry between the western and eastern Pacific in $4\times\text{CO}_2$ is mostly resolved in G1, the
27 tropical Pacific is overall wetter under $4\times\text{CO}_2$ but drier in G1.

28 **3.1.3 Zonal wind stress**

29 Changes in zonal wind stress are directly dependent on and interact with ENSO amplitude
30 (Guilyardi, 2006), ENSO period (Zelle et al., 2005; Capotondi et al., 2006), and ZSSTG (Hu
31 and Fedorov, 2016). A positive feedback loop between zonal wind stress, SST, and
32 | thermocline depth influences the evolution of ENSO (Philip and van Oldenborgh, 2006). A
33 decrease in the strength of the trade winds is concurrent with a flattening of the thermocline,
34 a reduction of upwelling in the eastern Pacific, and increased SST in the eastern relative to
35 the western equatorial Pacific, thus resulting in further weakening of the trade winds (Collins
36 et al., 2010). We use the zonal wind stress index, Westerly Wind Bursts (WWBs), and
37 Easterly Wind Bursts (EWBs) to study the wind stress over the tropical Pacific. The zonal
38 wind stress index is defined as the wind stress averaged over the equatorial tropical Pacific
39 | ($5^\circ \text{ N}\text{-}5^\circ \text{ S}$; $120^\circ \text{ E}\text{-}80^\circ \text{ W}$), ~~whereas selecting only~~. ~~Although here not explicitly diagnosed~~
40 ~~through daily data, WWBs and EWBs are contained respectively in the positive {and~~
41 ~~negative} values of the ~~this~~ wind stress ~~over the same region defines the WWBs (EWBs)~~~~

1 [\(index \(see Hu and Fedorov, 2016\). As the duration of WWBs is 5 to 40 days \(Gebbie et al.,](#)
2 [2007\), the monthly mean data of westerly wind stress includes a monthly average of these](#)
3 [bursts.](#)

4 We find that the zonal wind stress is significantly reduced over most parts of the tropical
5 Pacific, especially over the Niño3 region in both 4×CO₂ and G1 (Fig. 3a-e), in agreement
6 with the reduced zonal SST gradients in both scenarios (Fig. 1). The zonal wind stress
7 weakens by 31-% and 10-% in 4×CO₂ and G1 (statistically significant at 99-% cl; Fig. 4a),
8 respectively. We also see a considerable weakening of zonal wind stress over the Niño3
9 region, both under 4×CO₂ and G1. The strength of WWBs increases by 13-% under G1
10 relative to piControl (99 % cl), while the EWBs decrease in strength by 7-% (99-% cl). In
11 comparison, the strength of both the WWBs and EWBs is reduced (99-% cl) under 4×CO₂, by
12 33-% and 28-%, respectively. The strong WWBs are more closely linked to positive SST
13 anomalies than negative SST anomalies (Cai et al., 2015a) and thus are likely to increase the
14 frequency of extreme El Niño events (Hu and Fedorov 2016) in G1, which is important with
15 regards to the mechanistic interpretation of the ENSO changes below.

16 3.1.4 Zonal and meridional sea surface temperature gradients

17 The ZSSTG between western and eastern equatorial Pacific is one of the characteristic
18 features of the equatorial tropical Pacific. The ZSSTG is weak during an El Niño and strong
19 during La Niña events (Latif et al., 2009). The ZSSTG is calculated as the difference between
20 SST in the western Pacific Warm Pool (5° N-5° S; 100° E-126° E) and eastern equatorial
21 Pacific (Niño3 region: 5° N-5° S; 160° E-150° W). The zonal SST gradient is reduced both in
22 4xCO₂ and G1 (Fig. 4b, 99-% cl), but the reduction is smaller in G1 (11-%) than in 4xCO₂
23 (62-%). The reduced zonal SST asymmetry in 4×CO₂ and G1 is consistent with the
24 weakening of the trade winds and zonal wind stress, as noted in Sect. 3.1.3. The weakening
25 of trade winds can result in reduced upwelling in the eastern equatorial Pacific, and east to
26 west surface currents (Collins et al., 2010), leading to an increase in El Niño events. Our
27 results under 4xCO₂ are in agreement with Coats and Karnauskas (2017), who using several
28 climate models found a weakening of the ZSSTG under the RCP8.5 scenario.

29 MSSTG is calculated as the SST averaged over the off-equatorial region (5° N-10° N; 150°
30 W-90° W) minus SST averaged over the equatorial region (2.5° N-2.5° S; 150° W-90° W) (Cai
31 et al., 2014). Reversal of sign or weakening of the MSSTG has been observed during extreme
32 El Niño events, as the ITCZ moves over the equator (e.g., Cai et al., 2014). Overall there is a
33 change in sign and reduction of MSSTG in 4×CO₂ (~-111-%, 99-% cl) and only [a slight](#)
34 [decrease](#) in G1 (~-9-%, 99-% cl) (Fig. S3, and Table S2). The decrease in strength of MSSTG
35 is an indication that extreme El Niño events are expected to increase (Cai et al., 2014) under
36 solar geoengineering. The weakening of the MSSTG is qualitatively in agreement with
37 previous studies under increased GHG forcings (e.g., Cai et al., 2014; Wang et al., 2017).

38 3.1.5 Thermocline

39 Previous studies (e.g., Vecchi and Soden, 2007; Yeh et al., 2009) revealed shoaling as well as
40 a reduction in the east-west tilt of the equatorial Pacific thermocline under increased GHG

1 scenarios. A decrease in thermocline depth and slope is a dynamical response to reduced
2 zonal wind stress. Shoaling of the equatorial Pacific thermocline can result in positive SST
3 anomalies in the eastern tropical Pacific, which in turn can affect the formation of El Niño
4 (Collins et al., 2010).

5 Thermocline depth here is defined as the depth of the 20 °C (for piControl and G1), and 24 °C
6 (for 4×CO₂) isotherms averaged between 5° N and 5° S, following Phillip and van
7 Oldenborgh (2006). Due to surface warming in GHG scenarios, the 20 °C isotherm deepens
8 (Yang and Wang et al., 2009), and this must be compensated by using a warmer isotherm (24
9 °C) as a metric in the 4×CO₂ case.

10 In 4xCO₂, the tropical Pacific thermocline depth (24 °C isotherm) shoals by 22-% (99-% cl,
11 Fig. 4c), as expected from similar experiments (Vecchi and Soden, 2007; Yeh et al., 2009).
12 However, there is no statistically significant change in the mean thermocline depth in G1. In
13 4xCO₂, most likely the weakened easterlies (as noticed in Sect. 3.1.3; e.g., Yeh et al., 2009,
14 Wang et al., 2017) and greater ocean temperature stratification due to increased surface
15 warming (see Sect. 4 and Cai et al., 2018) lead to a significant shoaling of the thermocline
16 across the western and central equatorial Pacific. In contrast, relatively little change takes
17 place between 130° W and 90° W. In a CMIP3 multimodel (SRESA1B scenario) ensemble,
18 Yeh et al. (2009) found a more profound deepening of the thermocline in this part of the
19 eastern equatorial Pacific; however, for example, Nowack et al. (2017) did not find such
20 changes under 4xCO₂ (cf. their Fig. S9). One possible explanation for this behaviour is the
21 competing effects of upper-ocean warming (which deepens the thermocline) and the
22 weakening of westerly zonal wind stress, causing thermocline shoaling (see Kim et al.
23 2011a).

24 3.1.6 Vertical velocity and Walker circulation

25 Under normal conditions, there is strong atmospheric upwelling over the western equatorial
26 Pacific, SPCZ, and ITCZ. In contrast, the relatively cold and dry eastern Pacific is dominated
27 by atmospheric downwelling. This process, as simulated in HadCM3L, can be seen in maps
28 of Omega500-100 (Fig. 5a). The region of ascent over the SPCZ and ITCZ moves
29 equatorward in 4×CO₂ (Fig 5b), consistent with the increase in SST and precipitation over the
30 equatorial region (Fig. 1d and 2d). The convective centre also moves towards the Niño3
31 region and centres at ~~~150°W~~ 150° W. While these changes in spatial patterns of atmospheric
32 divergence and convergence are found to be corrected for G1 (Fig. 5c), significant
33 differences in the strength of the atmospheric circulation remain, which in turn are coupled to
34 the aforementioned changes in atmospheric stability. Specifically, both for 4×CO₂ and G1,
35 upwelling decreases over the Warm Pool, but increases in the central Pacific and the eastern
36 part of the Niño3 region (Fig. 5d-e). This picture is consistent with changes in the spatial
37 extent and a weakening of the tropical PWC (Fig. 6a-c). In 4xCO₂, the weakening and
38 shifting of circulation patterns are consistent with multimodel results reported by Bayr et al.
39 (2014) under GHG forcing. While mitigated, the PWC weakening found in G1 remains
40 highly statistically significant (99-% cl; Fig. 6d-e).

1
2
3
4
5
6
7
8
9
10
11
12
13
14
15
16
17
18
19
20
21
22
23
24
25
26
27
28
29
30
31
32
33
34
35
36
37
38

3.2 ENSO amplitude and frequency

In Sect. 3.1, we described a variety of coupled, and highly significant changes in the tropical Pacific mean state, such as the weakening of zonal and meridional SST gradients, zonal wind stress, and PWC. It is well-known that such changes can affect ENSO variability. This section discusses various metrics used to ~~eharacterize~~~~characterise~~ ENSO variability and unfolds how they change in 4xCO₂ and G1. Specifically, we investigate the amplitude of ENSO, changes in amplitude asymmetry between El Niño and La Niña events, and ENSO frequency.

3.2.1 ENSO amplitude

To ~~eharacterize~~~~characterise~~ changes in ENSO, this study uses two separate indices for two different regions, because extreme warm and cold events are not mirror images of each other (Cai et al., 2015b). The Niño3 (Niño4) index is employed for studying characteristics of El Niño (La Niña) events in the eastern (central) Pacific region. ENSO amplitude is defined as the standard deviation of SST anomalies in a given ENSO region (e.g., Philip and van Oldenborgh 2006; Nowack et al., 2017). The maximum amplitude of warm events is defined as the maximum positive ENSO anomaly during the entire time series analysed (Gabriel and Robock, 2015). Cold events are defined similarly, but using the maximum negative ENSO anomaly.

In 4xCO₂, both eastern and central Pacific ENSO amplitudes undergo a statistically significant decrease (47 and 64%, respectively, at 99% cl, Table 1-2). The maximum amplitude of warm events in the eastern Pacific and cold events in the central Pacific are also significantly reduced (57% and 36% at 99% cl, respectively; Table 3-4). Previous studies found that climate models produced mixed responses (both increases and decreases in amplitude) in terms of how ENSO amplitude change with global warming (see Latif et al., 2009; Collins et al., 2010; Vega-Westhoff and Sriver, 2017). However, Cai et al. (2018) found an intermodel consensus, for models capable of ~~reproduceingsimulating~~ ENSO diversity, for strengthening of ENSO amplitude under A2, RCP4.5, and RPC8.5 transient scenarios. In contrast, in G1, the eastern Pacific ENSO amplitude gets strengthened (9% at 99% cl), and no statistically significant change is noticed in the central Pacific ENSO amplitude.

Further, the maximum amplitude of cold events is strengthened in the central Pacific (20% at 99% cl), but no statistically significant change occurs in the eastern Pacific. A validation of these changes in ENSO amplitude using the E- and C-indices, as these indices represent SST anomalies similar to those of Niño3 and Niño4 index (Cai et al., 2015a), yields indeed very ~~similar~~~~identical~~ results (see Table 1-4). Thus, our simulations imply that significant changes can occur in ENSO events under solar geoengineering. Mechanistically, it is self-evident that

1 these changes might be linked to the tropical Pacific SST overcooling of ca. 0.30 °C and the
2 substantial SST gradient changes under G1 relative to piControl.

3 However, the use of standard deviations to define ENSO amplitude is suboptimal, because
4 amplitudes of El Niño and La Niña events are asymmetric, i.e., in general, El Niño events are
5 stronger than La Niña events (An and Jin, 2004; Schopf and Burgman, 2006; Ohba and Ueda,
6 2009; Ham, 2017). The relative strength of ENSO warm and cold events can be measured by
7 the skewness of SST over the ENSO regions (Vega-Westhoff and Srivier, 2017). Following
8 Ham (2017), we investigate the asymmetry in the amplitude of El Niño and La Niña events
9 by comparing the skewness of detrended Niño3 SST anomalies in piControl with 4×CO₂ and
10 G1.

11 We find that, relative to piControl, the Niño3 SST skewness is reduced both in 4×CO₂ (190-%
12 at 99-% cl) and G1 (65-% at 99-% cl) (Table 5). The E-Index also indicates reduced skewness
13 under both 4×CO₂ (85-%) and G1 (28-%) at 99-% cl. The reduced skewness is further
14 illustrated in maps showing differences in skewness between 4×CO₂ and G1 with piControl
15 (Fig. S4). Over the eastern equatorial Pacific, the SSTs are transformed from positively to
16 negatively skewed under 4×CO₂ (Fig. S4b). Our results qualitatively agree with Ham (2017),
17 who found a 40-% reduction in ENSO amplitude asymmetry using several CMIP5 models in
18 the RCP4.5 scenario. In G1 (Fig. S4e), the skewness of SSTs is reduced over the eastern
19 equatorial Pacific, whereas it strengthens over the central equatorial Pacific region (at 99-%
20 cl). The strengthening of skewness over the central equatorial Pacific is also consistent with
21 increased C-Index skewness (66-% at 99-% cl) under G1 relative to piControl. Thus, due to
22 the concurrent strengthening of the maximum amplitude of cold events and reduction in the
23 asymmetry of SST skewness, the intensity of cold events is predicted to increase compared to
24 warm events under solar geoengineering.

25 3.2.2 El Niño frequency

26 ~~To study changes in El Niño frequency, we first need to define what constitutes an El Niño~~
27 ~~event. We here define~~ choose a threshold value of rainfall for defining extreme El Niño events
28 ~~as episodes when monthly mean~~ based on the work of Cai et al., (2014, 2017), who chose
29 ~~averaged~~ DJF Niño3 total rainfall ~~exceeds~~ exceeding 5 mm day⁻¹, ~~following the for this~~
30 ~~threshold definition by Cai et al. (2014) based on observations.~~ However, as pointed out by
31 Cai et al. (2017), trends in Niño3 rainfall are mainly driven by two factors: (1) the change in
32 the mean state of the tropical Pacific and (2) the change in frequency of extreme El Niño
33 events. Therefore, since we want to focus on the changes in the extremes, we need to remove
34 contribution (1) from the raw Niño3 time series. We, therefore, fit a quadratic polynomial to
35 the time series of rainfall data from which all extreme El Niño events (DJF total rainfall > 5
36 mm day⁻¹) have been excluded and then subtract this trend from the raw Niño3 rainfall time
37 series. Linearly detrending the rainfall time series produces similar results. Note that under
38 piControl (observations), total rainfall of 5 mm day⁻¹ is ~85th (~93rd) percentile in detrended
39 Niño3 rainfall time series. Wang et al. (2020) termed events with rainfall > 5 mm day⁻¹ as
40 extreme convective El Niño events.

1 With detrended Niño3 total rainfall exceeding 5 mm day⁻¹ as an extreme, three extreme and
2 seven moderate El Niño events can be identified from the historical record between 1979 and
3 2017 (Fig. 7a). A statistically significant increase of 526-% (99-% cl) in extreme El Niño
4 events can be seen under 4×CO₂ (939 events) relative to piControl (150 events) (Fig. 7b-c).
5 The geoengineering of climate (G1) largely offsets the increase in extreme El Niño frequency
6 under 4×CO₂ (Fig. 7d), however, compared to piControl, still a 17-% increase in extremes
7 and a 12-% increase in the total number of El Niño events (moderate plus extreme) can be
8 seen at 95-% cl. Thus, an El Niño event occurring every ~3.3-yr under preindustrial
9 conditions occurs every ~2.9-yr under solar geoengineered conditions.

10 A threshold of detrended Niño3 total rainfall of 5 mm day⁻¹ ~~recognizes~~recognises events as
11 extremes even when the MSSTG is positive and stronger, especially under 4×CO₂, which
12 plausibly means that ITCZ might not shift over the equator for strong convection to occur
13 during such extremes. The El Niño event of 2015 is a typical example of such events. We test
14 our results with a more strict criterion by choosing only those events as extremes, which have
15 characteristics similar to that of 1982 and 1997 El Niño events (i.e., Niño3 rainfall > 5 mm
16 day⁻¹ and MSSTG < 0). We declare events having characteristics similar to that of the 2015
17 event as moderate El Niño events (Fig. S5). Based on this method, we find a robust increase
18 in the number of extreme El Niño events both in 4×CO₂ (924-%) and G1 (61-%) at 99-% cl.
19 We also performed the same analysis by linearly detrending the rainfall time series and find
20 similar results (Fig. S6).

21 An alternative approach to quantifying extreme El Niño events is based on Niño3 SST index
22 > 1.75 s.d. as an extreme event threshold (Cai et al., 2014). We note that using this definition,
23 no statistically significant change in the number of extreme El Niño events is detected in G1
24 (61 events), whereas they reduced from 57 in piControl to zero events in 4×CO₂ highlighting
25 the dependency of specific results on the precise definition of El Niño events used. However,
26 relative to piControl, Niño3 SST index indicates a statistically significant increase (decrease)
27 of 12-% (46-%) in the frequency of the total number of El Niño events (Niño3 SST index >
28 0.5 s.d.) (Table S3) in G1 (4×CO₂). Further, we examine the change in extreme El Niño
29 events using E-Index > 1.5 s.d. (see Cai et al., 2018) as a threshold. The SST based E-Index
30 identifies 79, 147, and 93 extreme El Niño events in piControl, 4×CO₂, and G1, respectively.
31 Thus using E-Index, extreme El Niño events increase by 86-% (99-% cl) and 17-% (missing
32 95-% cl by three events) in 4×CO₂ and G1, respectively. Based on the E-index definition, we
33 ~~also~~ see a statistically significant increase in the total number of El Niño events in 4×CO₂
34 (~~88107%~~) and ~~G1 (12-%)~~no statistically significant change in G1 (Table S3). Note that Wang
35 et al. (2020) showed that extreme ~~convective~~El Niño events having E-Index > 1.5 s.d. can
36 still happen even if the ~~E-index~~Niño3 rainfall is not greater than 5 mm day⁻¹ (cf. Figure 2 in
37 Wang et al., 2020).

38 We highlight that both in 4×CO₂ and solar geoengineered climate, more weak and reversed
39 MSSTG events occur relative to piControl (Fig. S3). More frequent reversals of MSSTG
40 result in a more frequent establishment of strong convection in the eastern equatorial Pacific.
41 According to Cai et al. (2014), more frequent convection over the eastern tropical Pacific
42 increases the sensitivity of rainfall by 25-% to positive SST anomalies. Further, in Sect. 3.1.3,

1 | we found that WWBs (EWBs) are 13-% (7-%) stronger (weaker) than in piControl, which
2 | also favours a higher frequency of El Niño events in G1. Thus, we conclude that changes in
3 | the tropical Pacific mean state; in particular weakening of temperature gradients (MSSTG
4 | and ZSSTG), changes in zonal wind stress, and convection over the tropical Pacific (and
5 | consistent weakening of the PWC) are the plausible causes of increased frequency of extreme
6 | El Niño events under G1.

7 | 3.2.3 La Niña frequency

8 | During La Niña events, the ZSSTG, the PWC, and atmospheric convection in the western
9 | Pacific are stronger than on average. Here, we present plots of Niño4 vs ZSSTG for
10 | piControl, 4×CO₂, and G1 (Fig. 8a-c). In 4×CO₂, extreme La Nina events are reduced to zero
11 | relative to piControl, and a statistically significant (99-% cl) decrease occurs in moderate,
12 | weak, and total number (sum of extreme, moderate and weak events) of La Niña events. Our
13 | findings are inconsistent to those of Cai et al. (2015b) who found nearly doubling of extreme
14 | La Nina events under increased GHG forcing. We ~~find~~see a statistically significant (95-% cl)
15 | increase in extreme La Niña events in G1. The number of extreme La Niña events increases
16 | by 32-% (61 events) in G1 relative to piControl (46 events). Thus, an extreme La Niña event
17 | occurs every ~22 years in piControl and every ~16 years in G1.

18 | The increased number of extreme El Niño events provides a possible mechanism for
19 | increased frequency of La Niña events, as they result in more heat discharge events causing
20 | cooling, hence providing conducive conditions for increased occurrence of La Niña events
21 | (Cai et al., 2015a, 2015b). In addition, the ocean becomes 4% more stratified under G1
22 | relative to piControl (Fig. 15e, Table S7). The increased vertical ocean stratification in the
23 | central equatorial Pacific steers cooling in the Niño4 region and, hence, can cause more
24 | frequent strong positive ZSSTG anomalies (Fig. S9c and S10b) resulting in an increased
25 | number of extreme La Niña events (see also Cai et al., 2015b).

26 | 3.3 Spatial characteristics of ENSO

27 | In Sect. 3.2, we showed that overall and maximum ENSO event amplitudes generally
28 | strengthened under G1, while the amplitude asymmetry between warm and cold events is
29 | significantly reduced. In this section, we present composite anomalies, i.e. the average
30 | patterns of all El Niño and La Niña events. These composites provide process-based evidence
31 | for the strengthening (weakening) of extreme La Niña (El Niño) events in G1. We show that
32 | the PWC, SST, and composite rainfall anomalies are strengthened for extreme La Niña
33 | events, while they are weakened for extreme El Niño events under G1. For composite
34 | analysis, extreme El ~~Niño~~Niño events are selected with Niño3 rainfall > 5 mm day⁻¹ and
35 | MSSTG < 0 (Fig. S5) because it gives a more robust estimate as all events show a reversal of
36 | MSSTG and more vigorous convection.

37 | 3.3.1 Weakening of extreme El Niño events in G1

38 | The broad spatial patterns of composite SST (Fig. 9), rainfall (Fig. 10), and PWC (Fig. 11)
39 | anomalies for the extreme and total number of El Niño events in G1 are very similar to those

1 of piControl. During extreme El Niño events, in G1, we find reduced SST (Fig. 9e) and
2 rainfall anomalies (Fig. 10e) over the eastern and western equatorial Pacific with a consistent
3 weakening of the eastern and western branch of PWC (Fig. 11e). We also note reduced SST
4 (Fig. 9f) and rainfall (Fig. 10f) anomalies over the western Pacific in agreement with a
5 weakening of western branch of PWC (Fig. 11f) for the total number of El Niño events in G1.
6 Thus, in general, extreme El Niño events tend to be weaker in G1 than in piControl. We
7 conclude that, in our simulations, extreme El Niño events are more frequent but slightly less
8 intense in a solar geoengineered climate than in preindustrial conditions. We further confirm
9 this with a histogram of detrended Niño3 SST anomalies (Fig. S7a). Though more frequent
10 positive Niño3 SST anomalies occur under G1 (between 1 and 3 °C), the mean Niño3 SST
11 anomaly is weaker in G1 (1.95 °C) than in piControl (2.23 °C) at 99-% cl. Thus, the strength
12 of extreme El Niño events is reduced by ~12-% in G1 compared to piControl. However, no
13 statistically significant shift in histograms of Niño3 SST anomalies is detected for the total
14 number of El Niño events (Fig. S7b).

15 **3.3.2 Strengthening of La Niña events in G1**

16 The broad spatial patterns of composite SST (Fig 12a-d), rainfall (Fig. 13a-d) and PWC (14a-
17 d) anomalies for the extreme and total number of La Niña events are similar under G1 and
18 piControl. During the extreme and total number of La Niña events, the negative SST and
19 rainfall anomalies, and both east and west branch of PWC are strengthened indicating an
20 overall intensification of La Niña events in G1 relative piControl. We note that most of the
21 stronger negative SST anomalies occur over the eastern equatorial Pacific. We confirm
22 strengthening of La Niña events by plotting histograms of detrended Niño3 SST anomalies
23 for the extreme (piControl: -1.45 °C; G1: -1.68 °C) and the total number of La Niña events
24 (piControl: -1.03 °C; G1: -1.22 °C) based on the Niño4 SST index (Fig. S7c-d). Thus, we
25 conclude that the strength of extreme (total number of) La Niña events is increased by ~16-%
26 (~18-%) in G1 compared to piControl.

27 **4 Mechanisms behind the changes in ENSO variability**

28 **4.1 Under greenhouse gas forcing**

29 The reduced ENSO amplitude under 4×CO₂ is mainly caused by stronger hf and weaker BJ
30 feedback relative to piControl (Fig. 15a-b, and Table S5-6). More rapid warming over the
31 eastern than western equatorial Pacific regions reduces the SST asymmetry between western
32 and eastern Pacific (Fig. 1d), resulting in the weakening of ZSSTG (Fig. 4b) that significantly
33 weakens the zonal winds stress (Fig. 4a) and hence PWC (Fig. 6b, d, see Bayr et al., 2014).
34 The overall reduction of zonal wind stress reduces the BJ feedback, which, in turn, can
35 weaken the ENSO amplitude. Climate models show an inverse relationship between hf
36 feedback and ENSO amplitude (Lloyd et al., 2009, 2011; Kim and Jin, 2011b). The increased
37 hf feedback might be the result of enhanced clouds due to strengthened convection (Fig. 5b,
38 d) and stronger evaporative cooling in response to enhanced SSTs under 4×CO₂ (Knutson
39 and Manabe, 1994; Kim and Jin, 2011b). Kim and Jin (2011a, b) found intermodel consensus
40 on the strengthening of hf feedback in CMIP3 models under enhanced GHG warming

1 | scenario (Ferret and Collins, 2019). Further, we see increased ocean stratification under
2 | 4×CO₂ (Fig. 15d and Table S7). A more stratified ocean is associated with an increase in both
3 | the El Niño events and amplitude in the eastern Pacific (Wang et al., 2020). It can also
4 | modify the balance between feedback processes (Dewitte et al., 2013). Enhanced
5 | stratification may also cause negative temperature anomalies in the central to the western
6 | Pacific through changes in thermocline tilt (Dewitte et al., 2013). Since the overall ENSO
7 | amplitude decreases in our 4×CO₂ simulation, we, thus, conclude that the ocean stratification
8 | mechanisms cannot be the dominant factor here, but that hf and BJ feedbacks must more than
9 | cancel out the effect of ocean stratification on ENSO amplitude. Bjerknes feedback is a
10 | multi-component process (e.g., Kim and Jin, 2011a), where some components may increase
11 | and some may decrease under the influence of external forcing. For instance, increased upper
12 | ocean stratification tends to enhance the Bjerknes feedback, likely through coupling between
13 | the wind and thermocline. However, this study represents the Bjerknes feedback solely on the
14 | coupling between wind and SST, a caveat of this analysis.

15 | The increased frequency of extreme El Niño events under 4×CO₂ is due to change in the
16 | mean position of the ITCZ (Fig. S2), causing frequent reversals of MSSTG (Fig. S3), and
17 | eastward extension of the western branch of PWC (Fig. 6), which both result in increased
18 | rainfall over the eastern Pacific (see Wang et al., 2020). This is due to greater east equatorial
19 | than off-equatorial Pacific warming (see Cai et al., 2020), which shifts the mean position of
20 | ITCZ towards the equator (Fig. S2). Simultaneously more rapid warming of the eastern than
21 | western equatorial Pacific reduces the ZSSTG, and hence zonal wind stress, as also evident
22 | from the weakening and shift of the PWC (Fig. 6) and increased instances of negative ZSSTG
23 | anomalies (Fig. S9). Ultimately, this leads to more frequent vigorous convection over the
24 | Niño3 region (Fig. 5d), and enhanced rainfall (Fig. 2d, S8). Therefore, despite the weakening
25 | of the ENSO amplitude under 4×CO₂, rapid warming of the eastern equatorial Pacific causes
26 | frequent reversals of meridional and zonal SST gradients, resulting in an increased frequency
27 | of extreme El Niño events (see also Cai et al., 2014; Wang et al., 2020).

28 | We note that under GHG forcing, HadCM3L does not simulate an increase in the frequency
29 | of extreme La Niña events as found by Cai et al. (2015b) using CMIP5 models. However, it
30 | does show an increase in the total number of La Niña events (Table S4). In a multimodel
31 | ensemble mean, Cai et al. (2015b) found that the western Pacific warms more rapidly than
32 | the central Pacific under increased GHG forcing, resulting in strengthening of the zonal SST
33 | gradient between these two regions. Strengthening of this zonal SST gradient and increased
34 | vertical upper ocean stratification provide conducive conditions for increased frequency of
35 | extreme La Niña events (Cai et al., 2015b). One reason why we do not see an increase in the
36 | frequency of central Pacific extreme La Niña events might be that HadCM3L does not
37 | simulate more rapid warming of the western Pacific compared to the central Pacific as
38 | noticed by Cai et al. (2015b) (compare our Fig. 1d with Fig. 3b in Cai et al., 2015b), hence, as
39 | stronger zonal SST gradient does not develop, across the equatorial Pacific, as needed for
40 | extreme La Niña events to occur (see Fig. S9a, c and S10).

41 | **4.2 Under solar geoengineering**

1 G1 over cools the upper ocean layers, whereas the GHG-induced warming in the lower ocean
2 layers is not entirely offset, thus increasing ocean stratification (Fig. 15). The increased
3 stratification boosts atmosphere-ocean coupling (see Cai et al., 2018), which favours
4 enhanced westerly wind bursts (Fig. 4a) (e.g., Capotondi et al., 2018) to generate stronger
5 SST anomalies over the eastern Pacific (Wang et al., 2020). The larger cooling of the western
6 Pacific than the eastern Pacific can also enhance westerly wind bursts reinforcing the BJ
7 feedback and hence SST anomalies in the eastern Pacific. We conclude that increased ocean
8 stratification, along with stronger BJ feedback, is the most likely mechanism behind the
9 overall strengthening of ENSO amplitude under G1.

10 The increased frequency of extreme El Niño events under G1 can be linked to the changes in
11 MSSTG and ZSSTG (see Cai et al., 2014, and Fig. S3, S9). The eastern off-equatorial Pacific
12 cools more than the eastern equatorial regions, providing relatively more conducive
13 conditions for convection to occur through a shift of ITCZ over to the Niño3 region (Fig. 1e).
14 At the same time, the larger cooling of the western equatorial Pacific than of the eastern
15 equatorial Pacific reduces the ZSSTG and convective activity over the western Pacific, which
16 leads to a weakening of the western branch of PWC (Fig. 6e). Hence we see reduced rainfall
17 over the western Pacific and enhanced rainfall from the Niño3 to the central Pacific region
18 (Fig 2e). These mean state changes, strengthening of convection between $\sim 140^\circ$ W and $\sim 150^\circ$
19 E, and more reversals of the MSSTG and ZSSTG (Fig. S3) result in an increased number of
20 extreme El Niño events in G1 than in piControl (Fig. 7).

21 5 Discussion and conclusions

22 In this paper, we have ~~analyzed~~ **analysed** the impact of abruptly increased GHG forcing
23 ($4\times\text{CO}_2$), and solar geoengineering (G1), on the tropical Pacific mean climate and ENSO
24 extremes. Previous solar geoengineering studies did not show any statistically significant
25 change in the PWC (e.g., Guo et al., 2018) or ENSO frequency and amplitude (e.g., Gabriel
26 and Robock 2015). However, those results were strongly limited by the length of the
27 respective simulations, which made changes challenging to detect, given the high tropical
28 Pacific climate variability. This limitation has been overcome here by using long (1000-year)
29 climate model simulations, carried out with HadCM3L. The longer record makes it possible
30 to detect even relatively small changes between the preindustrial and G1 scenarios within the
31 chosen model system.

32 To conclude, solar geoengineering can compensate many of the GHG-induced changes in the
33 tropical Pacific, but, importantly, not all of them. In particular, controlling the downward
34 shortwave flux cannot correct one of the climate system's most dominant modes of
35 variability, i.e., ENSO, wholly back to preindustrial conditions. The ENSO feedbacks
36 (Bjerkness and heat flux) and more stratified ocean temperatures may induce ENSO to
37 behave differently under G1 than under piControl and $4\times\text{CO}_2$. Different meridional
38 distributions of shortwave and longwave forcings (e.g., Nowack et al., 2016) resulting in the
39 surface ocean overcooling, and residual warming of the deep ocean are the plausible reasons
40 for the solar geoengineered climate not reverting entirely to the preindustrial state. ~~However~~

1 The changes in ENSO feedbacks and more stratified ocean temperatures under both 4×CO₂
2 and G1 can also affect the eastern and central Pacific ENSO variability differently. For
3 instance, more stratified ocean and enhanced BJ feedback in G1 strengthens the eastern
4 Pacific ENSO amplitude but not central Pacific ENSO amplitude (Table 1-2). Similarly, the
5 enhanced hf and weaker BJ feedback in 4×CO₂ results in a more substantial reduction in
6 central Pacific ENSO amplitude than eastern Pacific ENSO amplitude (Table 1-2). In the
7 current model system, we expect that changes in tropical Pacific mean state and feedback
8 process, both under 4×CO₂ and G1, may impact the occurrence ratio of central Pacific El
9 Niño (La Niña) to eastern Pacific El Niño (La Niña) (e.g., Yeh et al., 2009), which requires
10 further detailed analysis.

11 Finally, we note that this is a single model study, and more studies are needed to show the
12 robustness and model-dependence of any results discussed here, e.g. using long-term
13 multimodel ensembles from GeoMIP6 (Kravitz et al., 2015), once the data are released. The
14 long-term Stratospheric Aerosol Geoengineering Large Ensemble (GLENS; Tilmes et al.,
15 2018) data can also be explored to investigate ENSO variability under geoengineering.

16 We summarizesummarise our key findings as follows:

- 17 1. The warming over the tropical Pacific under increased GHG forcing (4×CO₂) is
18 overcompensated under solar sunshade geoengineering (G1), resulting, by design, in
19 tropical mean overcooling of approximately 0.3 °C. This overcooling is more
20 pronounced in the western tropical Pacific and SPCZ than in the eastern Pacific under
21 the G1 scenario.
- 22 2. The reduced SST and rainfall asymmetry between the warm pool and the cold tongue,
23 seen under 4×CO₂, is mostly corrected in G1, but regionally important differences
24 remain relative to preindustrial conditions. The tropical Pacific is 5-% wetter in
25 4×CO₂, whereas it is 5-% drier in G1 relative to piControl. In particular, solar
26 geoengineering results in decreased rainfall over the warm pool, SPCZ, and ITCZ and
27 increased rainfall over the central and eastern equatorial Pacific.
- 28 3. The preindustrial median position of ITCZ (154° W-82° W; 7.5° N) changes
29 significantly under 4×CO₂ and moves over the equator (154° W-82° W; 0°). G1
30 restores the ITCZ to its preindustrial position (154° W-82° W; 7.5° N).
- 31 4. The increased GHG forcing results in 31-% reduction in zonal wind stress over the
32 tropical Pacific. G1 fails to compensate this reduction entirely and results in
33 weakening the zonal wind stress by 10-% with a 13-% (7-%) increase (decrease) in
34 WWBs (EWBs), thus providing more conducive conditions for El Niño extremes.
- 35 5. Under solar geoengineering, both ZSSTG and MSSTG are reduced by 11-% and 9-%,
36 respectively. More frequent reversal of MSSTG occurs in G1 relative to piControl.
- 37 6. In 4×CO₂, the thermocline flattens over the tropical Pacific, and G1 recovers its
38 preindustrial condition.
- 39 7. The PWC becomes weaker both under 4×CO₂ and G1 scenarios.
- 40 8. The increased GHG forcing results in a weakening of ENSO amplitude, whereas solar
41 geoengineering strengthens it relative to preindustrial climate. The maximum
42 amplitude of cold events is enhanced under G1.

- 1 9. The reduced ENSO amplitude under $4\times\text{CO}_2$ is mainly due to enhanced hf feedback,
2 whereas the increase under G1 is mainly caused by enhanced BJ feedback and ocean
3 stratification.
- 4 10. The ENSO amplitude asymmetry between warm and cold events is reduced under G1
5 relative to piControl.
- 6 11. The frequency of extreme El Niño events increases by 61% in G1 relative to
7 piControl. Further, the frequency of the total number of El Niño events also increases
8 by 12%. Thus, an El Niño event occurring every ~3.3-yr under preindustrial
9 conditions occurs every ~2.9-yr under solar geoengineered climate. The reason for the
10 occurrence of more extreme El Niño events under G1 is more frequent reversals of
11 MSSTG compared to piControl.
- 12 12. The frequency of extreme La Niña events increases by 32% under G1 relative to
13 piControl. Thus, an extreme La Niña event occurring every ~22-yr in piControl
14 occurs every ~16-yr in G1.

15 **Author contribution.** Long Cao developed the model code and performed the simulations.
16 Abdul Malik formulated the research questions, defined the methodology with the help of all
17 co-authors, and performed the scientific analysis. Abdul Malik prepared the manuscript with
18 contributions from all co-authors.

19 **Competing interests.** The authors declare that they have no conflict of interest.

20 **Data availability.** Data are available upon request from Long Cao (longcao@zju.edu.cn).

21 **Acknowledgments**

22 **Acknowledgements**

23

24 The Swiss National Science Foundation supported this work under the grant EarlyPostdoc.
25 Mobility (P2BEP2_175255). Peer J. Nowack ~~is~~was funded through an Imperial College
26 Research Fellowship. The authors thank the referees for their comments and suggestions,
27 which have much helped us to improve our manuscript. GPCP Precipitation and NCEP
28 Reanalysis data ~~was~~were provided by the NOAA/OAR/ESRL PSD, Boulder, Colorado, USA,
29 from their Web site at <https://www.esrl.noaa.gov/psd/>. The ERA5 data was downloaded from
30 <https://cds.climate.copernicus.eu/cdsapp#!/home>.

31 **References**

- 32
- 33
- 34 Adler, R. F., Huffman, G. J., Chang, A., Ferraro, R., Xie, P-P., Janowiak, J., Rudolf, B.,
35 Schneider, U., Curtis, S., Bolvin, D., Gruber, A., Susskind, J., Arkin, P., and Nelkin, E.:
36 The version-2 Global Precipitation Climatology Project (GPCP) monthly precipitation
37 analysis (1979–Present), *J. Hydrometeorol.*, 4, 1147–1167, [https://doi.org/10.1175/1525-7541\(2003\)004<1147:TVGPCP>2.0.CO;2](https://doi.org/10.1175/1525-7541(2003)004<1147:TVGPCP>2.0.CO;2), 2003.
- 38
- 39 An, S-II., and Jin, F-F.: Nonlinearity and Asymmetry of ENSO, *J. Climate.*, 17, 2399–2412,
40 [https://doi.org/10.1175/1520-0442\(2004\)017<2399:NAAOE>2.0.CO;2](https://doi.org/10.1175/1520-0442(2004)017<2399:NAAOE>2.0.CO;2), 2004.

Formatted: Font: Not Bold, English (U.K.)

Formatted: Normal, Left

Formatted: Font: 10 pt, English

- 1 Bala, G., Duffy, P. B., and Taylor, K. E.: Impact of geoengineering schemes on the global
2 hydrological cycle. *Proc. Natl. Acad. Sci. U. S. A.*, 105, 7, 664–7, 669,
3 <https://doi.org/10.1073/pnas.0711648105>, 2008.
- 4 Bayr, T., Dommenges, D., Martin, T., [and](#) Power, S. B.: The eastward shift of the Walker
5 circulation in response to global warming and its relationship to ENSO variability. *Clim.
6 Dyn.*, 43, 2747–2763, <https://doi.org/10.1007/s00382-014-2091-y>, 2014.
- 7 Bellenger, H., Guilyardi, E., Leloup, J., Lengaigne, M., [and](#) Vialard, J.: ENSO representation
8 in climate models: from CMIP3 to CMIP5. *Clim. Dyn.*, 42, 1999–2018, <http://doi.org/10.1007/s00382-013-1783-z>, 2014.
- 10 Boer, G. J., Yu, B., Kim, S., [and](#) Flato, G. M.: Is there observational support for an El Niño-
11 like pattern of future global warming? *Geophys. Res. Lett.*, 31, 1–4,
12 <https://doi.org/10.1029/2003GL018722>, 2004.
- 13 Bove, M. C., Elsner, J. B., Landsea, C. W., Niu, X., [and](#) O'Brien, J. J.: Effect of El Niño on
14 U.S. landfalling hurricanes, revisited, *B. Am. Meteorol. Soc.*, 79 (11), 2477–2482,
15 [https://doi.org/10.1175/1520-0477\(1998\)079<2477:EOENOO>2.0.CO;2](https://doi.org/10.1175/1520-0477(1998)079<2477:EOENOO>2.0.CO;2), 1998.
- 16 Cai, W., Borlace, S., Lengaigne, M., van Rensch, P., Collins, M., Vecchi, G., Timmermann,
17 A., Santoso, A., McPhaden, M. J., Wu, L., England, M. H., Wang, G., Guilyardi, E., and
18 Jin, F-F.: Increasing frequency of extreme El Niño events due to greenhouse warming,
19 *Nat. Clim. Change.*, 4(2), 111–116, <https://doi.org/10.1038/nclimate2100>, 2014.
- 20 Cai, W., Santoso, A., Wang, G., Yeh, S. W., An, S. I., Cobb, K. M., Collins, M., Guilyardi,
21 E., Jin, F-F., Kug, J-S., Lengaigne, M., McPhaden, M. J., Takahashi, K., Timmermann,
22 A., Vecchi, G., Watanabe, M., and Wu, L.: ENSO and greenhouse warming. *Nat. Clim.
23 Change.*, 5(9), 849–859. <https://doi.org/10.1038/nclimate2743>, 2015a.
- 24 Cai, W., Wang, G., Dewitte, B., Wu, L., Santoso, A., Takahashi, K., Yang, Y., Carréric, A.,
25 [and](#) McPhaden, M. J.: Increased variability of eastern Pacific El Niño greenhouse
26 warming. *Nature*, 564, 201–206, <https://doi.org/10.1038/s41586-018-0776-9>, 2018.
- 27 Cai, W., Wang, G., Santoso, A., Lin, X., and Wu, L.: Definition of Extreme El Niño and Its
28 Impact on Projected Increase in Extreme El Niño Frequency. *Geophys. Res. Lett.*,
29 44(21), 11184–11190, <https://doi.org/10.1002/2017GL075635>, 2017.
- 30 Cai, W., Wang, G., Santoso, A., McPhaden, M. J., Wu, L., Jin, F-F., Timmermann, A.,
31 Collins, M., Vecchi, G., Lengaigne, M., England, M. H., Dommenges, D., Takahashi,
32 K., and Guilyardi, E.: Increased frequency of extreme La Niña events under greenhouse
33 warming, *Nat. Clim. Change.*, 5(2), 132–137, <https://doi.org/10.1038/nclimate2492>,
34 2015b.
- 35 Cao, L., Duan, L., Bala, G., and Caldeira, K.: Simulated long-term climate response to
36 ~~idealized~~[idealised](#) solar geoengineering, *Geophys. Res. Lett.*, 43(5), 2209–2217,
37 <https://doi.org/10.1002/2016GL068079>, 2016.
- 38 Capotondi, A., Wittenberg, A., [and](#) Masina, S.: Spatial and temporal structure of Tropical
39 Pacific interannual variability in 20th century coupled simulations, *ocean. Model.*, 15(3-
40 4), 274–298, <https://doi.org/10.1016/j.ocemod.2006.02.004>, 2006.
- 41 Chen, L., Li, T., Yu, Y., and Behera, S. K.: A possible explanation for the divergent
42 projection of ENSO amplitude change under global warming, *Clim. Dynam.*, 49(11–12),
43 3799–3811, <https://doi.org/10.1007/s00382-017-3544-x>, 2017.

- 1 | Chung, C. T. Y., Power, S. B., Arblaster, J. M., Rashid, H. A., and Roff, G. L.: Non-linear
2 | precipitation response to El Niño and global warming in the Indo-Pacific. *Clim. Dyn.*,
3 | 42, 1837–1856, <https://doi.org/10.1007/s00382-013-1892-8>, 2014.
- 4 | Coats, S., and Karnauskas, K. B.: Are Simulated and Observed Twentieth-Century Tropical
5 | Pacific Sea Surface Temperature Trends Significant Relative to Internal Variability?
6 | *Geophys. Res. Lett.*, 44, 9928–9937, <https://doi.org/10.1002/2017GL074622>, 2017.
- 7 | Collins, M., An, S.-I., Cai, W., Ganachaud, A., Guilyardi, E., Jin, F.-F., Jochum, M.,
8 | Lengaigne, M., Power, S., Timmermann, A., Vecchi, G., and Wittenberg, A.: The
9 | impact of global warming on the tropical Pacific Ocean and El Niño. *Nature*
10 | *Geoscience*, 3(6), 391–397, <https://doi.org/10.1038/ngeo868>, 2010.
- 11 | Copernicus Climate Change Service (C3S): ERA5: Fifth generation of ECMWF atmospheric
12 | reanalyses of the global climate. Copernicus Climate Change Service Climate Data Store
13 | (CDS), January 2020. <https://cds.climate.copernicus.eu/cdsapp#!/home>,
14 | <https://doi.org/10.24381/cds.f17050d7>, 2017.
- 15 | Cox, P. M., Betts, R. A., Jones, C. D., Spall, S. A., and Totterdell, I. J.: Acceleration of global
16 | warming due to carbon-cycle feedbacks in a coupled climate model, *Nature*,
17 | <https://doi.org/10.1038/35041539>, 2000.
- 18 | Crutzen, P. J: Albedo enhancement by stratospheric sulfur injections: A contribution to
19 | resolve a policy dilemma?, *Climatic Change*, 77(3–4), 211–219,
20 | <https://doi.org/10.1007/s10584-006-9101-y>, 2006.
- 21 | Curry, C. L., Sillmann, J., Bronaugh, D., Alterskjaer, K., Cole, J. N. S., Ji, D., Kravitz, B.,
22 | Kristjánsson, J. E., Moore, J. C., Muri, H., Niemeier, U., Robock, A., Tilmes, S., and
23 | Yang, S.: A multimodel examination of climate extremes in an idealizedidealised
24 | geoengineering experiment, *J. Geophys. Res-Atmos.*, 119(7), 3900–3923,
25 | <https://doi.org/10.1002/2013JD020648>, 2014.
- 26 | Dewitte, B., Yeh, S.-W., and Thual, S.: Reinterpreting the thermocline feedback in the
27 | western-central equatorial Pacific and its relationship with the ENSO modulation. *Clim*
28 | *Dyn*, 41, 819–830, <https://doi.org/10.1007/s00382-012-1504-z>, 2013.
- 29 | Essery, R., and Clark, D. B.: Developments in the MOSES 2 land-surface model for PILPS
30 | 2e, *Global Planet. Change.*, 38(1-2), 161–164, [https://doi.org/10.1016/S0921-](https://doi.org/10.1016/S0921-8181(03)00026-2)
31 | [8181\(03\)00026-2](https://doi.org/10.1016/S0921-8181(03)00026-2), 2003.
- 32 | Ferret, S., and Collins, M.: ENSO feedbacks and their relationships with the mean state
33 | in a flux adjusted ensemble. *Clim. Dyn.*, 52, 7189–7208, [https://doi.org/10.1007/s00382-](https://doi.org/10.1007/s00382-016-3270-9)
34 | [016-3270-9](https://doi.org/10.1007/s00382-016-3270-9), 2019.
- 35 | Gabbie, G., Eisenman, I., Wittenberg, A., and Tziperman, E.: Modulation of Westerly Wind
36 | Bursts by Sea Surface Temperature: A Semistochastic Feedback for ENSO. *J. Atmos.*
37 | *Sci.*, 64 (9), 3281–3295, <https://doi.org/10.1175/JAS4029.1>, 2007.
- 38 | Gabriel, C. J., and Robock, A.: Stratospheric geoengineering impacts on El Niño/Southern
39 | Oscillation, *Atmos. Chem. Phys.*, 15(20), 11949–11966, [https://doi.org/10.5194/acp-15-](https://doi.org/10.5194/acp-15-11949-2015)
40 | [11949-2015](https://doi.org/10.5194/acp-15-11949-2015), 2015.
- 41 | Gandhi, S. M., and Sarkar, B. C.: Conventional and Statistical Resource/Reserve Estimation,
42 | in: *Essentials of Mineral Exploration and Evaluation*, Elsevier, 1st Edition, 271–288,
43 | <https://doi.org/10.1016/C2015-0-04648-2>, 2016.

Formatted: Font color: Red

- 1 Gibbons, J. D., and Chakraborti, S.: Nonparametric Statistical Inference, 5th Ed., Statistics:
2 Textbooks & Monographs, Chapman and Hall/CRC Press, Taylor and Francis Group,
3 2011.
- 4 Govindasamy, B., [and](#) Caldeira, K.: Geoengineering Earth's radiation balance to mitigate
5 CO₂-induced climate change, *Geophys. Res. Lett.*, 27(14), 2141-2144,
6 <https://doi.org/10.1029/1999GL006086>, 2000.
- 7 Guilyardi, E.: El Niño–mean state–seasonal cycle interactions in a multimodel ensemble,
8 *Clim. Dynam.*, 26(4), 329-348, <https://doi.org/10.1007/s00382-005-0084-6>, 2006.
- 9 Guo, A., Moore, J. C., and Ji, D.: Tropical atmospheric circulation response to the G1
10 sunshade geoengineering radiative forcing experiment, *Atmos. Chem. Phys.*, 18, 8689-
11 8706, <https://doi.org/10.5194/acp-18-8689-2018>, 2018.
- 12 Ham, Y.: A reduction in the asymmetry of ENSO amplitude due to global warming: The role
13 of atmospheric feedback, *Geophys. Res. Lett.*, 44(16), 8576–8584,
14 <https://doi.org/10.1002/2017GL074842>, 2017.
- 15 Hollander, M., and Wolfe D. A.: Non-parametric Statistical Methods, 2nd Ed., John Wiley
16 and Sons, Inc., 1999.
- 17 Hong, Y., Moore J. C., Jevrejeva, S., Ji, D., Phipps, S. J., Lenton, A., Tilmes, S., Watanabe,
18 S., and Zhao, L.: Impact of the GeoMIP G1 sunshade geoengineering experiment on the
19 Atlantic meridional overturning circulation, *Environ. Res. Lett.*, 12(3),
20 <https://doi.org/10.1088/1748-9326/aa5fb8>, 2017.
- 21 Hu, S., and Fedorov, A. V.: Exceptionally strong easterly wind burst stalling El Niño of 2014,
22 *P. Natl. Acad. Sci. USA.*, 113(8), 2005-2010, <https://doi.org/10.1073/pnas.1514182113>,
23 2016.
- 24 Huang, P., and Ying, J.: A multimodel ensemble pattern regression method to correct the
25 tropical pacific SST change patterns under global warming. *J. Climate.*, 28(12), 4706–
26 4723, <https://doi.org/10.1175/JCLI-D-14-00833.1>, 2015.
- 27 [Kao, H.-Y., and Yu, j.-Y.: Contrasting Eastern-Pacific and Central-Pacific Types of ENSO. *J.*](#)
28 [Climate](#), 22(3), 615–632, <https://doi.org/10.1175/2008JCLI2309.1>, 2009.
- 29 Kim, S. T., Cai, W., Jin, F.-F., Santoso, A., Wu, L., Guilyardi, E., and An, S.-I.: Response of
30 El Niño sea surface temperature variability to greenhouse warming. *Nat. Clim. Change.*,
31 4(9), 786–790, <https://doi.org/10.1038/nclimate2326>, 2014.
- 32 Kim, S. T., [and](#) Jin, F.-F.: An ENSO stability analysis. Part I: results from a hybrid
33 coupled model. *Clim Dyn.*, 36, 1593–1607, <https://doi.org/10.1007/s00382-010-0796-0>,
34 2011a.
- 35 Kim, S. T., [and](#) Jin, F.-F.: An ENSO stability analysis. Part II: results from the twentieth
36 and twenty-first century simulations of the CMIP3 models. *Clim Dyn.*, 36, 1609–1627,
37 <https://doi.org/10.1007/s00382-010-0872-5>, 2011b.
- 38 Knutson, T. R., [and](#) Manabe, S.: Impact of increased CO₂ on simulated ENSO-like
39 phenomena. *Geophys. Res. Lett.*, 21, 2295-2298, <https://doi.org/10.1029/94GL02152>,
40 1994.
- 41 Kohyama, T., Hartmann, D. L., and Battisti, D. S.: La Niña-like mean-state response to
42 global warming and potential oceanic roles, *J. Climate.*, 30(11), 4207–4225,
43 <https://doi.org/10.1175/JCLI-D-16-0441.1>, 2017.

- 1 Kravitz, B., Caldeira, K., Boucher, O., Robock, A., Rasch, P. J., Alterskjær, K., Karam, D.
2 B., Cole, J. N. S., Curry, C. L., Haywood, J. M., Irvine, P. J., Ji, D., Jones, A.,
3 Kristjánsson, J. E., Lunt D. J., Moore, J. C., Niemeier, U., Schmidt, H., Schulz, M.,
4 Singh, B., Tilmes, S., Watanabe, S., Yang, S., [and](#) Yoon, J-H.: Climate model response
5 from the Geoengineering Model Intercomparison Project (GeoMIP), *J. Geophys. Res-*
6 *Atmos.*, 118, 8320–8332, <https://doi.org/10.1002/jgrd.50646>, 2013b.
- 7 Kravitz, B., Forster, P. M., Jones, A., Robock, A., Alterskjær, K., Boucher, O., Jenkins, A. K.
8 L., Korhonen, H., Kristjánsson, J. E., Muri H., Niemeier, U., Partanen, A-I., Rasch, P. J.,
9 Wang, H., [and](#) Watanabe, S.: Sea spray geoengineering experiments in the
10 geoengineering model intercomparison project (GeoMIP): Experimental design and
11 preliminary results, *J. Geophys. Res-Atmos.*, 118(19), 11175–11186,
12 <https://doi.org/10.1002/jgrd.50856>, 2013a.
- 13 Kravitz, B., Robock, A., Boucher, O., Schmidt, H., Taylor, K. E., Stenchikov, G., and Schulz,
14 M.: The Geoengineering Model Intercomparison Project (GeoMIP), *Atmos. Sci. Lett.*,
15 12(2), 162–167, <https://doi.org/10.1002/asl.316>, 2011.
- 16 Kravitz, B., Robock, A., Tilmes, S., Boucher, O., English, J. M., Irvine, P. J., Jones, A.,
17 Lawrence, M. G., MacCracken, M., Muri, H., Moore, J. C., Niemeier, U., Phipps, S. J.,
18 Sillmann, J., Storelvmo, T., Wang, H., and Watanabe, S.: The Geoengineering Model
19 Intercomparison Project Phase 6 (GeoMIP6): simulation design and preliminary results,
20 *Geosci. Model Dev.*, 8, 3379–3392, <https://doi.org/10.5194/gmd-8-3379-2015>, 2015.
- 21 Latif, M., and Keenlyside, N. S.: El Niño/Southern Oscillation response to global warming,
22 *P. Natl. Acad. Sci. USA.*, 106 (49), 20578–20583, 10.1073/pnas.0710860105, 2009.
- 23 Liu, Z., Vavrus, S., He, F., Wen, N., and Zhong, Y.: Rethinking tropical ocean response to
24 global warming: The enhanced equatorial warming. *J. Climate.*, 18(22), 4684–4700,
25 <https://doi.org/10.1175/JCLI3579.1>, 2005.
- 26 Lloyd, J., Guilyardi, E., [and](#) Weller, H.: The role of atmosphere feedbacks during ENSO in
27 the CMIP3 models. Part II: using AMIP runs to understand the heat flux feedback
28 mechanisms. *Clim. Dyn.*, 37,1271–1292, <https://doi.org/10.1007/s00382-010-0895-y>,
29 2011.
- 30 Lloyd, J. E., Guilyardi, E., Weller, H., [and](#) Slingo, J.: The role of atmosphere feedbacks
31 during ENSO in the CMIP3 models *Atmos. Sci. Lett.*, 10, 170–176,
32 <https://doi.org/10.1002/asl.227170-176>, 2009.
- 33 Lunt, D. J., Ridgwell, A, Valdes, P. J., [and](#) Seale, A.: Sunshade World: A fully coupled GCM
34 evaluation of the climatic impacts of geoengineering, *Geophys. Res. Lett.*, 35(L12710),
35 <https://doi.org/10.1029/2008GL033674>, 2008.
- 36 Luo, Y., Lu, J., Liu, F., and Liu, W.: Understanding the El Niño-like oceanic response in the
37 tropical Pacific to global warming, *Clim. Dynam.*, 45(7–8), 1945–1964,
38 <https://doi.org/10.1007/s00382-014-2448-2>, 2015.
- 39 Malik, A., Brönnimann, S., Stickler, A., Raible, C. C., Muthers, S., Anet, J., Rozanov, E., [and](#)
40 Schmutz, W.: Decadal to multi-decadal scale variability of Indian summer monsoon
41 rainfall in the coupled ocean-atmosphere-chemistry climate model SOCOL-MPIOM,
42 *Clim. Dynam.*, 49(9–10), 3551–3572, <https://doi.org/10.1007/s00382-017-3529-9>, 2017.
- 43 Meehl G. A., [and](#) Washington, W. M.: El Niño like climate change in a model with increased
44 atmospheric CO2 concentrations, *Nature*, 382, 1996.

- 1 Moore, T. R., Matthews, H. D., Simmons, C., and Leduc, M.: Quantifying changes in
2 extreme weather events in response to warmer global temperature, *Atmos. Ocean.*,
3 53(4), 412–425, <https://doi.org/10.1080/07055900.2015.1077099>, 2015.
- 4 Nowack, P. J., Abraham, N. L., Braesicke, P., and Pyle, J. A.: Stratospheric ozone changes
5 under solar geoengineering: implications for UV exposure and air quality, *Atmos.*
6 *Chem. Phys.*, 16, 4191–4203, <https://doi.org/10.5194/acpd-15-31973-2015>, 2016.
- 7 Nowack, P. J., Abraham, N. L., Braesicke, P., and Pyle J. A.: The impact of stratospheric
8 ozone feedbacks on climate sensitivity estimates, *J. Geophys. Res. Atmos.*, 123, 4630–
9 4641, <https://doi.org/10.1002/2017JD027943>, 2018.
- 10 Nowack, P. J., Abraham, N. L., Maycock, A. C., Braesicke, P., Gregory, J. M., Joshi, M. M.,
11 Osprey, A., and Pyle, J. A.: A large ozone-circulation feedback and its implications for
12 global warming assessments, *Nat. Clim. Chang.*, 5(1), 41–45,
13 <https://doi.org/10.1038/nclimate2451>, 2015.
- 14 Nowack, P. J., Braesicke, P., Abraham, N. L., and Pyle J. A.: On the role of ozone feedback
15 in the ENSO amplitude response under global warming, *Geophys. Res. Lett.*, 44, 3858–
16 3866, <https://doi.org/10.1002/2016GL072418>, 2017.
- 17 Ohba, M., [and](#) Ueda H.: Role of non-linear atmospheric response to SST on the asymmetric
18 transition process of ENSO, 177–192. <https://doi.org/10.1175/2008JCLI2334.1>, 2009.
- 19 Pachauri, R. K., Allen, M. R., Barros, V. R., Broome, J., Cramer, W., Christ, R., Church, J.
20 A., Clarke, L., Dahe, Q., Dasgupta, P., Dubash, N. K., Edenhofer, O., Elgizouli, I., Field,
21 C. B., Forster, P., Friedlingstein, P., Fuglestvedt, J., Gomez-Echeverri, L., Hallegatte, S.,
22 Hegerl, G., Howden, M., Jiang, K., Jimenez Cisneroz, B., Kattsov, V., Lee, H., Mach, K.
23 J., Marotzke, J., Mastrandrea, M. D., Meyer, L., Minx, J., Mulugetta, Y., O'Brien, K.,
24 Oppenheimer, M., Pereira, J. J., Pichs-Madruga, R., Plattner, G. K., Pörtner, H. O.,
25 Power, S. B., Preston, B., Ravindranath, N. H., Reisinger, A., Riahi, K., Rusticucci, M.,
26 Scholes, R., Seyboth, K., Sokona, Y., Stavins, R., Stocker, T. F., Tschakert, P., van
27 Vuuren, D., and van Ypserle, J. P.: Climate change 2014: synthesis report, contribution
28 of Working Groups I, II and III to the Fifth Assessment Report of the Intergovernmental
29 Panel on Climate Change, Pachauri, R., and Meyer, L., (Eds.) , Geneva, Switzerland,
30 IPCC, 151 p., ISBN: 978-92-9169-143-2, 2014.
- 31 Park, W., Keenlyside, N., Latif, M., Ströh, A., Redler, R., Roeckner, E., and Madec, G.:
32 Tropical Pacific climate and its response to global warming in the Kiel Climate Model.
33 *J. Climate.*, 22(1), 71–92, <https://doi.org/10.1175/2008JCLI2261.1>, 2009.
- 34 Philip, S. Y., and van Oldenborgh, G. J.: Shifts in ENSO coupling processes under global
35 warming, *Geophys. Res. Lett.*, 33(11), 1–5, <https://doi.org/10.1029/2006GL026196>,
36 2006.
- 37 Power, S., Delage, F., Chung, C., Kociuba, G., [and](#) Keay, K.: Robust twenty-first-century
38 projections of El Niño and related precipitation variability. *Nature*, 502, 541–545,
39 <https://doi.org/10.1038/nature12580>, 2013.
- 40 Rayner, N. A., Parker, D. E., Horton, E. B., Folland, C. K., Alexander, L. V, Rowell, D. P.,
41 [and](#) Kaplan, A.: Global analyses of sea surface temperature, sea ice, and night marine
42 air temperature since the late nineteenth century, *J. Geophys. Res-Atmos.*, 108(D14),
43 <https://doi.org/10.1029/2002JD002670>, 2003.

- 1 Ropelewski, C. F., and Halpert, M. S.: Global and regional scale precipitation patterns
2 associated with the El Niño/Southern Oscillation, *Mon Weather Rev.*,
3 [https://doi.org/10.1175/1520-0493\(1987\)115<1606:GARSPP>2.0.CO;2](https://doi.org/10.1175/1520-0493(1987)115<1606:GARSPP>2.0.CO;2), 1987.
- 4 Santoso, A., Mcphaden, M. J., and Cai, W.: The defining characteristics of ENSO extremes
5 and the strong 2015/2016 El Niño, *Rev. Geophys.*, 55(4), 1079–1129,
6 <https://doi.org/10.1002/2017RG000560>, 2017.
- 7 Schmidt, H., Alterskjær, K., Alterskjær, K., Bou Karam, D., Boucher, O., Jones, A., ~~---~~and
8 Timmreck, C.: Solar irradiance reduction to counteract radiative forcing from a
9 quadrupling of CO₂: climate responses simulated by four earth system models, *Earth*
10 *Syst. Dynam.*, 3(1), 63–78, <https://doi.org/10.5194/esd-3-63-2012>, 2012.
- 11 Schopf, P. S., and Burgman R. J.: A simple mechanism for ENSO residuals and asymmetry,
12 *J. Climate.*, 19, 3167–3179, 2006.
- 13 Stevenson, S., and Fox-Kemper, B.: ENSO model validation using wavelet probability
14 analysis, *J. Climate.*, 23, 5540–5547, <https://doi.org/10.1175/2010JCLI3609.1>, 2010.
- 15 Stocker T. F., Qin D., Plattner, G. K., Tignor M., Allen, S. K., Boschung, J., Nauels, A., Xia,
16 Y., Bex, V., and Midgley P. M. (Eds.): Summary for Policymakers, in: *Climate Change*
17 *2013: The Physical Science Basis. Contribution of Working Group I to the Fifth*
18 *Assessment Report of the Intergovernmental Panel on Climate Change*, Cambridge
19 University Press, Cambridge, UK and New York, NY, USA,
20 <https://doi.org/10.1017/CBO9781107415324.004>, 2013.
- 21 Sun, N., Zhou, T., Chen, X., Endo, H., Kitoh, A., and Wu, B.: Amplified tropical Pacific
22 rainfall variability related to background SST warming. *Clim Dyn* 54, 2387–2402,
23 <https://doi.org/10.1007/s00382-020-05119-3>, 2020.
- 24 [Takahashi, K., Montecinos, A., Goubanova, K., and Dewitte, B.: ENSO regimes:
25 Reinterpreting the canonical and Modoki El Niño. *Geophys. Res. Lett.*, 38\(10\),
26 <https://doi.org/10.1029/2011GL047364>, 2011.](#)
- 27 Tilmes, S., Richter, J. H., Kravitz, B., MacMartin, D. G., Mills, M. J., Simpson, I. R.,
28 Glanville, A. S., Fasullo, J. T., Phillips, A. S., Lamarque, J., Tribbia, J., Edwards, J.,
29 Mickelson, S., and Gosh, S.: CESM1(WACCM) Stratospheric Aerosol Geoengineering
30 Large Ensemble (GLENS) Project. *Bull. Amer. Meteor. Soc.*, 99 (11), 2361–2371,
31 <https://doi.org/10.1175/BAMS-D-17-0267.1>, 2018.
- 32 Valdes, P. J., Armstrong, E., Badger, M. P. S., Bradshaw, C. D., Bragg, F., Crucifix, M.,
33 Davies-Barnard, T., Day, J. J., Farnsworth, A., Gordon, C., Hopcroft, P. O., Kennedy, A.
34 T., Lord, N. S., Lunt, D. J., Marzocchi, A., Parry, L. M., Pope, V., Roberts, W. H. G.,
35 Stone, E. J., Tourte, G. J. L., and Williams, J. H. T.: The BRIDGE HadCM3 family of
36 climate models: HadCM3@Bristol v1.0, *Geosci. Model Dev.*, 10, 3715–3743,
37 <https://doi.org/10.5194/gmd-10-3715-2017>, 2017.
- 38 van Oldenborgh, G. J., Philip, S. Y., and Collins, M.: El Niño in a changing climate: A
39 multimodel study, *ocean. Sci.*, 1(2), 81–95, <https://doi.org/10.5194/os-1-81-2005>, 2005.
- 40 Vecchi G. A., and Soden B. J., (2007). Global warming and the weakening of the tropical
41 circulation, *J. Climate.*, 20, 4316–4340, <https://doi.org/10.1175/JCLI4258.1>, 2007.
- 42 Vecchi, G. A., Soden, B. J., Wittenberg, A. T., Held, I. M., Leetmaa, A., and Harrison, M. J:
43 Weakening of tropical Pacific atmospheric circulation due to anthropogenic forcing,
44 *Nature*, 441, 73–76, <https://doi.org/10.1038/nature0474>, 2006.

- 1 Vecchi, G. A., and Wittenberg, A. T.: El Niño and our future climate: where do we stand?
2 Wiley Interdiscip. Rev. Clim. Chang., 1(2), 260–270, <https://doi.org/10.1002/wcc.33>,
3 2010.
- 4 Vega-Westhoff, B., and Srivler, R. L: Analysis of ENSO's response to unforced variability
5 and anthropogenic forcing using CESM, Scientific Reports, 7(1), 1–10,
6 <https://doi.org/10.1038/s41598-017-18459-8>, 2017.
- 7 Wang, G., Cai, W., and Santoso, A.: Stronger Increase in the Frequency of Extreme
8 Convective than Extreme Warm El Niño Events under Greenhouse Warming. J.
9 Climate, 33(2), 675–690, <https://doi.org/10.1175/JCLI-D-19-0376.1>, 2020.
- 10 Wang, G., Cai, W., Gan, B., Wu, L., Santoso, A., Lin, X., Chen, Z., and McPhaden, M. J.:
11 Continued increase of extreme El Niño frequency long after 1.5 C warming
12 stabilization-stabilisation. Nat. Clim. Change., 7(8), 568–572,
13 <https://doi.org/10.1038/NCLIMATE3351>, 2017.
- 14 Wang, Y., Luo, Y., Lu, J., and Liu, F.: Changes in ENSO amplitude under climate warming
15 and cooling, Clim. Dynam., 53–53. <https://doi.org/10.1007/s00382-018-4224-1>, 2018.
- 16 Watanabe, M., Kug, J-S., Jin, F-F., Collins, M., Ohba, M., and Wittenberg, A. T.: Uncertainty
17 in the ENSO amplitude change from the past to the future. Geophys. Res. Lett.,
18 39(L20703), <https://doi.org/10.1029/2012GL053305>, 2012.
- 19 Wigley, T., M., L.: A combined mitigation/geoengineering approach to climate
20 stabilization-stabilisation, Science, 314(5798), 452-454, [10.1126/science.1131728](https://doi.org/10.1126/science.1131728), 2006.
- 21 Xie, R., and Jin, F-F.: Two Leading ENSO Modes and El Niño Types in the Zebiak–Cane
22 Model. J. Climate, 31(5), 1943–1962, https://doi.org/10.1175/JCLI-D-17-0469.1, 2018.
- 23 Yang, H., and Wang F.: Revisiting the thermocline depth in the equatorial Pacific, J.
24 Climate., 22, 3856–3863, <https://doi.org/10.1175/2009JCLI2836.1>, 2009.
- 25 Yang, S., Li, Z., Yu, J.-Y., Hu, X., Dong, W., and He, S.: El Niño–Southern oscillation and
26 its impact in the changing climate, Natl Sci Rev, nwy046,
27 <https://doi.org/10.1093/nsr/nwy046>, 2018.
- 28 Yeh, S. W., Kug, J. S., Dewitte, B., Kwon, M. H., Kirtman, B. P., and Jin, F. F; El Niño in a
29 changing climate, Nature, 461(7263), 511–514, <https://doi.org/10.1038/nature08316>,
30 2009.
- 31 Yu, J-Y., and Kim, S. T.: Identification of Central-Pacific and Eastern-Pacific types of ENSO
32 in CMIP3 models. Geophys. Res. Lett., 37(15), https://doi.org/10.1029/2010GL044082,
33 2010.
- 34 Zelle, H., van Oldenborgh, G. J., Burgers, G., and Dijkstra, H.: El Niño and greenhouse
35 warming: results from ensemble simulations with the NCAR CCSM, J. Climate., 18,
36 4669-4683, <https://doi.org/10.1175/JCLI3574.1>, 2005.
- 37 Zhou, Z. Q., and Xie, S. P: Effects of climatological model biases on the projection of
38 tropical climate change, J. Climate., 28(24), 9909–9917, <https://doi.org/10.1175/JCLI-D-15-0243.1>, 2015.
- 39
40
41
42
43
44

1
2
3
4
5
6
7
8
9
10
11
12
13
14
15
16
17
18
19
20
21
22
23
24
25
26
27
28
29
30
31

Figures and Figure Captions

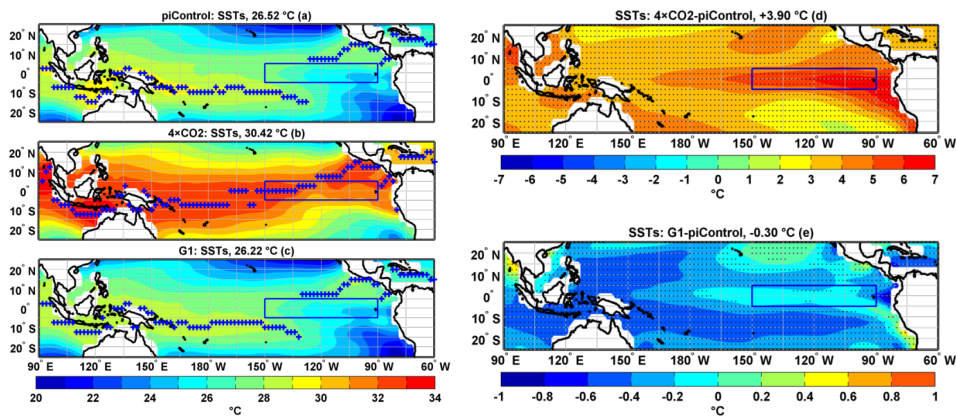


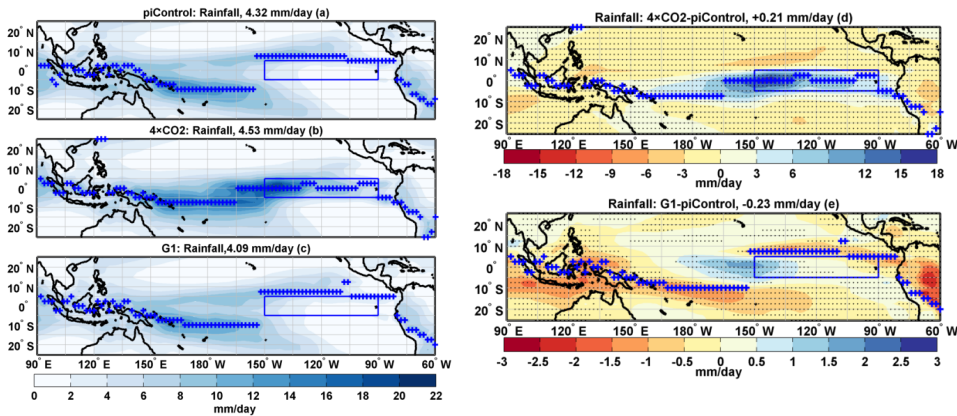
Figure 1. Tropical Pacific SST mean DJF climatology (a) piControl (b) $4\times\text{CO}_2$ (c) G1 (d) difference $4\times\text{CO}_2$ -piControl and (e) difference G1-piControl. The blue plus sign in a-c indicates latitudes with maximum SSTs. Stipples indicate grid points where the difference is statistically significant at 99-% cl using a non-parametric Wilcoxon rank-sum test. The box in the eastern Pacific identifies the Niño3 region. The numbers in a-c represent a mean temperature in the corresponding simulation, and numbers in d-e represent an area-averaged difference of piControl with $4\times\text{CO}_2$ and G1, respectively, in the tropical Pacific region (25°N - 25°S ; 90°E - 60°W).

Formatted: Indent: Left: 0 cm, First line: 0 cm, Line spacing: single

Formatted: Font: Bold

Formatted: Line spacing: single

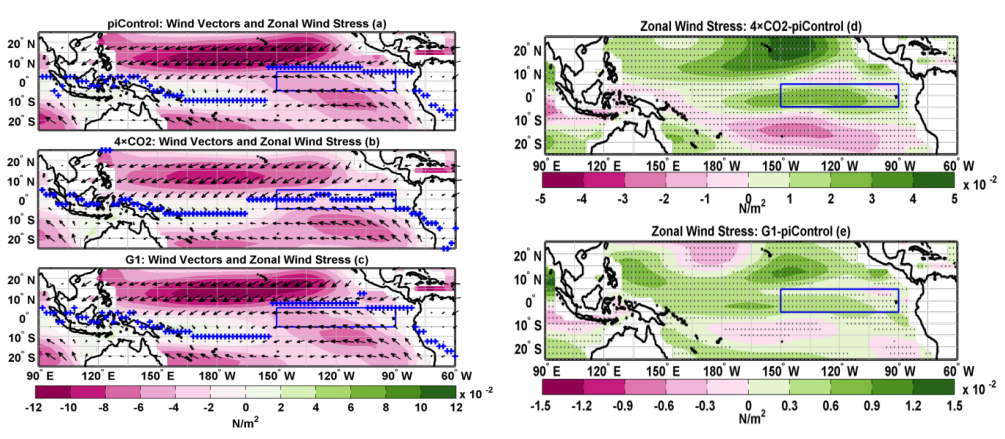
1
2
3
4



5

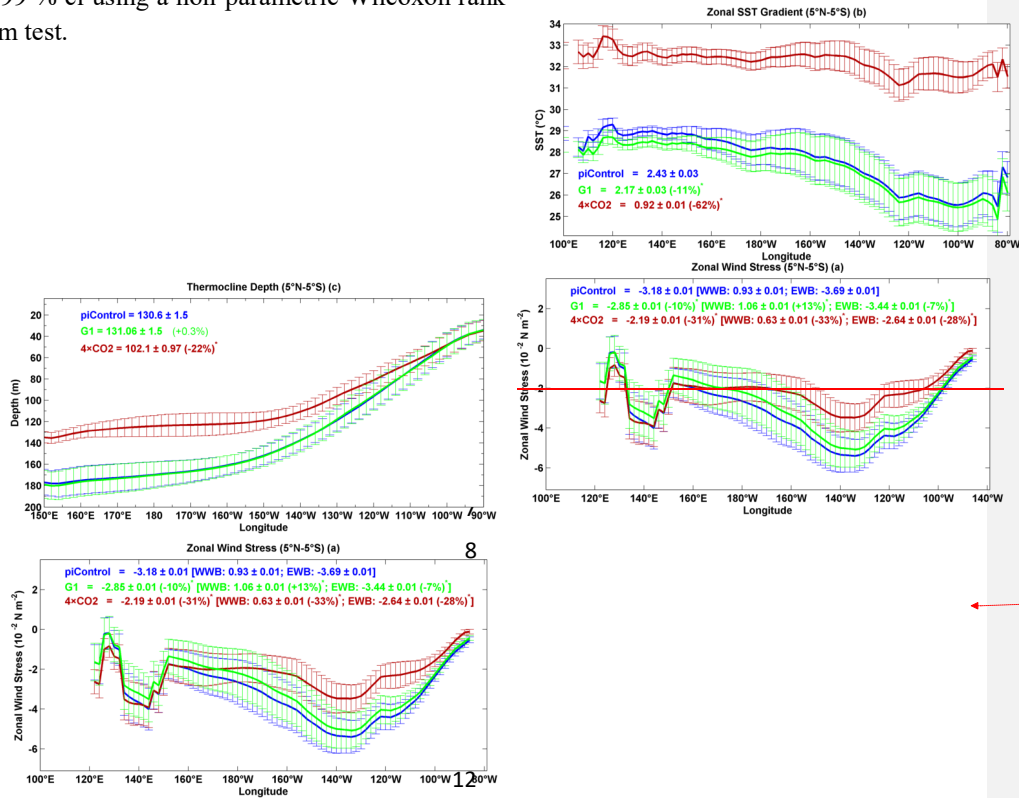
6 **Figure 2.** Tropical Pacific rainfall mean DJF climatology (a) piControl (b) $4\times\text{CO}_2$ (c) G1 (d)
7 difference: $4\times\text{CO}_2$ -piControl; the blue plus signs indicate the position of ITCZ under $4\times\text{CO}_2$
8 and (e) difference: G1-piControl; the blue plus signs indicate the position of ITCZ under G1.
9 In a-c, the blue plus signs indicate the position of ITCZ for the corresponding experiment.
10 Stipples indicate grid points where the difference is statistically significant at 99-% cl using a
11 non-parametric Wilcoxon rank-sum test. The numbers in a-c represent mean rainfall in the
12 corresponding simulation, and numbers in d-e represent an area-averaged difference of
13 piControl with $4\times\text{CO}_2$ and G1, respectively, in the tropical Pacific region (25°N - 25°S ; 90°E -
14 60°W).

15



16

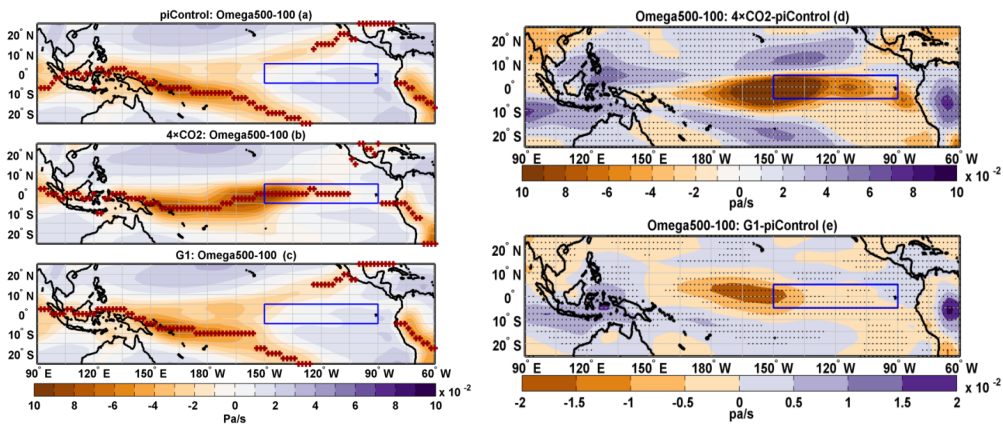
1 **Figure 3.** Tropical Pacific zonal wind stress mean DJF climatology (a) piControl (b) 4×CO₂
 2 (c) G1 (d) difference: 4×CO₂-piControl and (e) difference: G1-piControl. Black arrows
 3 indicate the direction of 10 m wind. The blue plus sign in a-c indicates latitudes with
 4 maximum rainfall. Stipples indicate grid points where the difference is statistically significant
 5 at 99-% cl using a non-parametric Wilcoxon rank-
 6 sum test.



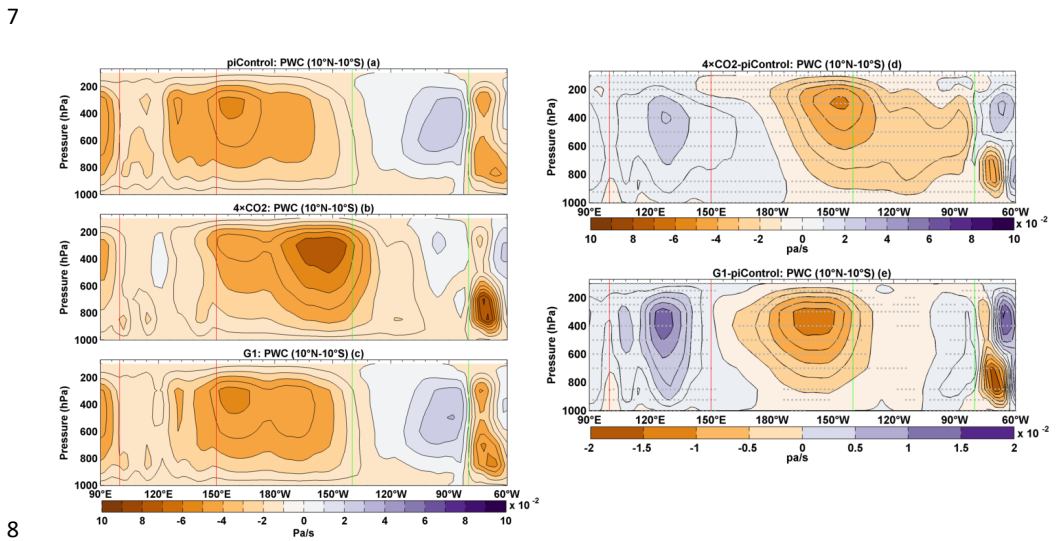
Formatted: Left

13
 14 **Figure 4.** DJF mean climatology of (a) zonal wind stress, (b) zonal SST gradient, and (c)
 15 thermocline depth. Error bars indicate ±1 s.d. calculated over the simulated period. Numbers
 16 with an asterisk indicate that the percentage change is statistically significant at 99-% cl.

17



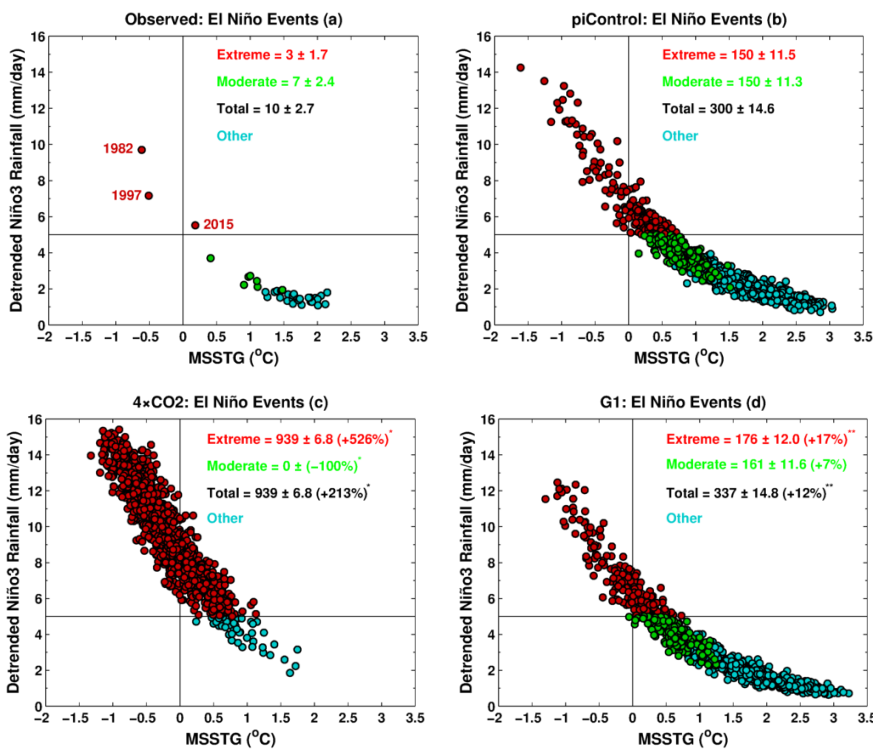
1
2 **Figure 5.** Tropical Pacific mean DJF climatology of vertical velocity averaged between 500-
3 and 100-hPa (Omega500-100) (a) piControl (b) 4×CO₂ (c) G1 (d) difference: 4×CO₂-
4 piControl and (e) difference: G1-piControl. In a-c, the brown plus sign indicates latitudes
5 where maximum upwelling occurs. Stipples indicate grid points where the difference is
6 statistically significant at 99-% cl using a non-parametric Wilcoxon rank-sum test.



8
9 **Figure 6.** Mean DJF climatology of tropical Pacific Walker Circulation averaged over 90° E-
10 60° W and 10° N-10° S (a) piControl (b) 4×CO₂ (c) G1 (d) difference: 4×CO₂-piControl and
11 (e) difference: G1-piControl. Green (red) vertical lines show the longitudinal spread of the
12 eastern (western) Pacific. Stipples indicate grid points where the difference is statistically
13 significant at 99-% cl using a non-parametric Wilcoxon rank-sum test.

14
15

1
2
3
4
5
6
7



8
9

10 **Figure 7.** Relationship between MSSTG and Niño3 rainfall for (a) observations (b) piControl
11 (c) 4xCO₂, and (d) G1. A solid black horizontal line indicates a threshold value of 5 mm day⁻¹. See text for the definition of extreme, moderate, and total El Niño events. A single (double)
12 asterisk indicates that the change in frequency, relative to piControl, is statistically significant
13 at 99-% (95-%) c.l. Numbers with a ± symbol indicate s.d. calculated with 10,000 bootstrap
14 realizationsrealisations. Following Cai et al. (2014), a non-ENSO related trend has been
15 removed from the rainfall time series.
16

17
18

1
2
3
4
5
6
7
8
9
10
11
12
13
14
15
16
17
18

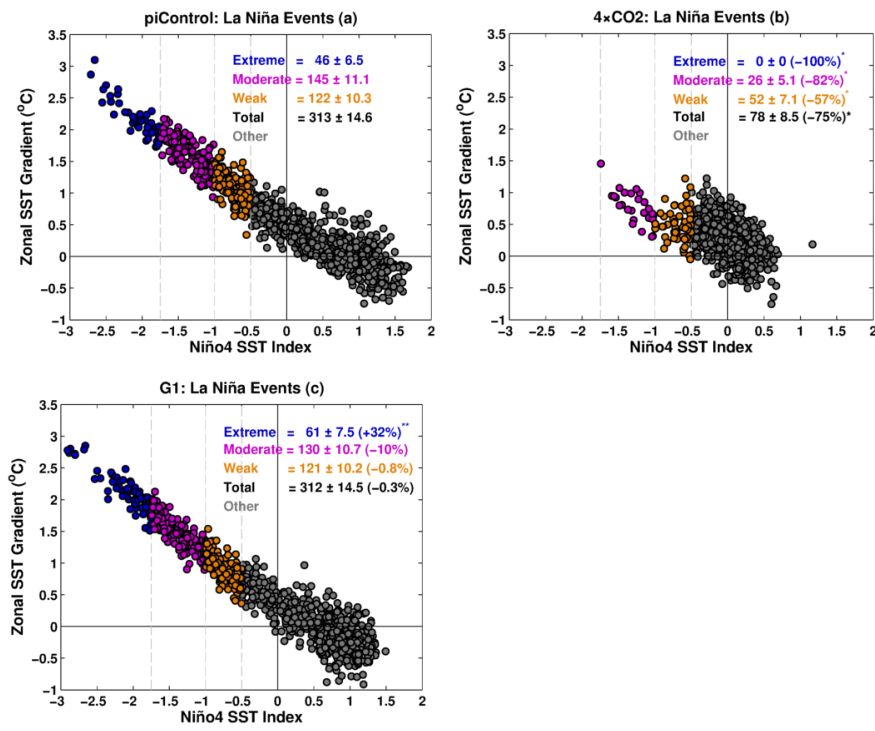


Figure 8. Relationship between ZSSTG and Niño4 SST index for (a) piControl (b) 4×CO₂ and (c) G1. Dashed grey vertical lines indicate threshold values of -1.75, -1, and -0.5 s.d. See text for the definition of extreme, moderate, weak, and total La Niña events. A single (double) asterisk indicates that the change in frequency is statistically significant at 99-% (95 %) cl. Numbers with a ± symbol indicate s.d. calculated with 10,000 bootstrap realizationsrealisations.

1
2
3
4
5
6
7
8
9
10
11
12
13
14
15
16
17
18
19
20
21

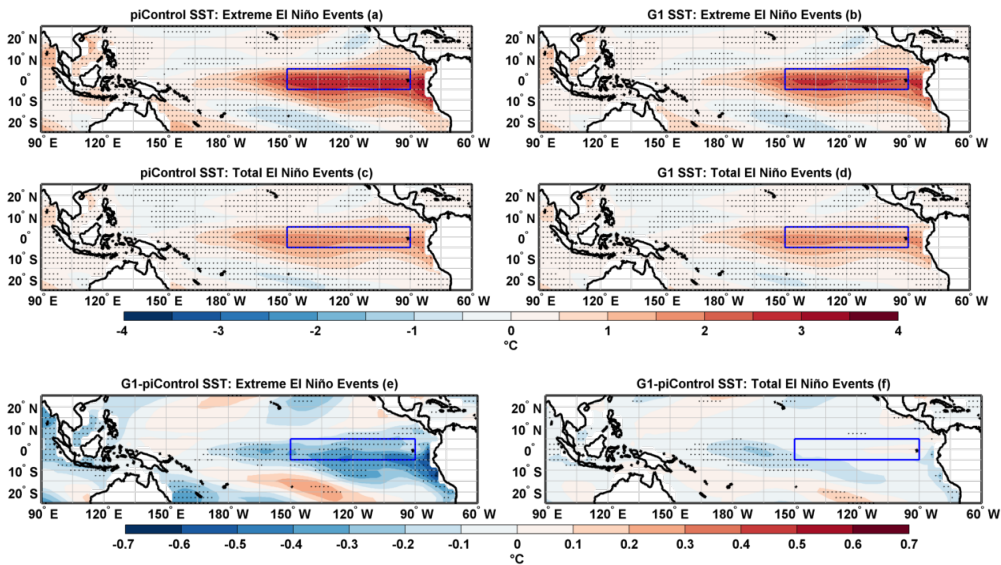


Figure 9. Composites of SST anomalies for extreme El Niño events in (a) piControl and (b) G1. Composites of SST anomalies for the total number of El Niño events in (c) piControl and (d) G1. Composite differences (G1-piControl) of SST anomalies for (e) extreme El Niño events and (f) total number of El Niño events. Stipples indicate grid points with statistical significance at 99-% cl using a non-parametric Wilcoxon rank-sum test. The blue box in the eastern Pacific identifies the Niño3 region.

1
2
3
4
5
6
7
8
9
10
11
12
13
14
15
16
17
18
19
20

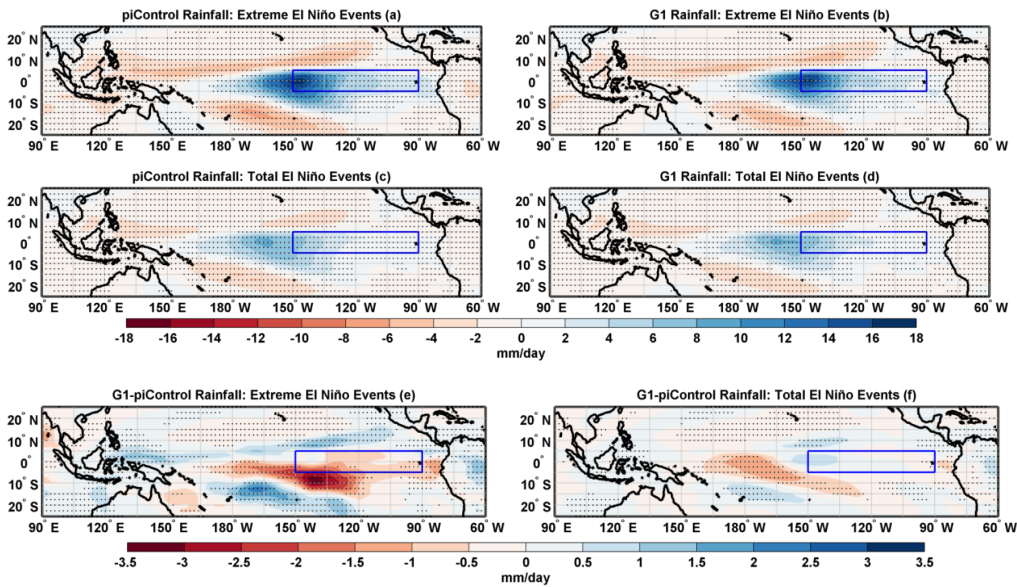


Figure 10. Composites of rainfall anomalies for extreme El Niño events in (a) piControl and (b) G1. Composites of rainfall anomalies for the total number of El Niño events in (c) piControl and (d) G1. Composite differences (G1-piControl) of rainfall anomalies for (e) extreme El Niño events and (f) total number of El Niño events. Stipples in a-d and f (e) indicate grid points with statistical significance at 99 (95) % cl using a non-parametric Wilcoxon rank-sum test. The blue box in the eastern Pacific identifies the Niño3 region.

1
2
3
4
5
6
7
8
9
10
11
12
13
14
15
16

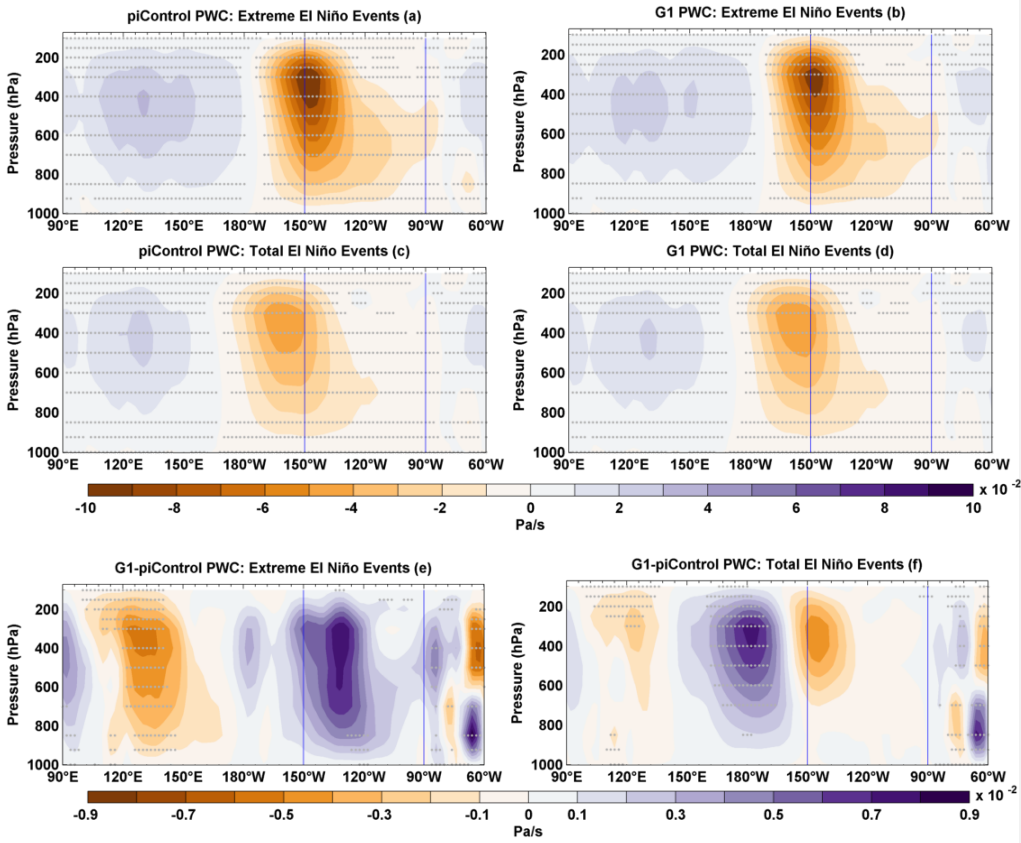
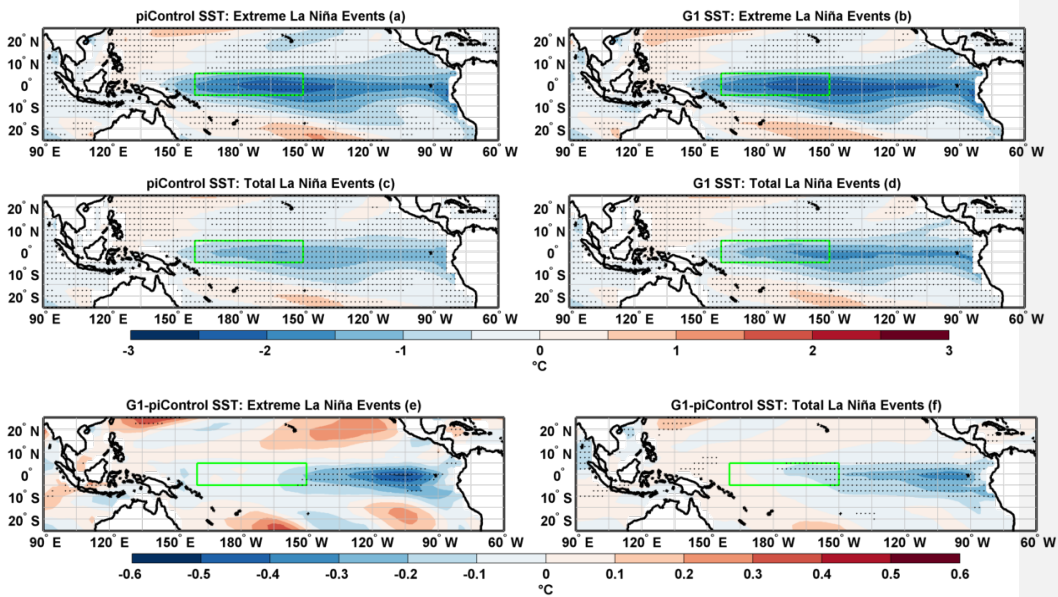


Figure 11. Composites of PWC anomalies for extreme El Niño events in (a) piControl and (b) G1. Composites of PWC anomalies for the total number of El Niño events in (c) piControl and (d) G1. Composite differences (G1-piControl) of PWC for (e) extreme El Niño events and (f) total number of El Niño events. Stipples indicate grid points with statistical significance at 99% CI using a non-parametric Wilcoxon rank-sum test. The blue vertical lines indicate the Niño3 region.



1

2

3 **Figure 12.** Composites of SST anomalies for extreme La Niña events in (a) piControl and (b)
 4 G1. Composites of SST for the total number of La Niña events in (c) piControl and (d) G1.
 5 Composite differences (G1-piControl) of SST for (e) extreme La Niña events and (f) the total
 6 number of La Niña events. Stipples indicate grid points with statistical significance at 99-% cl
 7 using a non-parametric Wilcoxon rank-sum test. The green box indicates the Niño4 region.

8

9

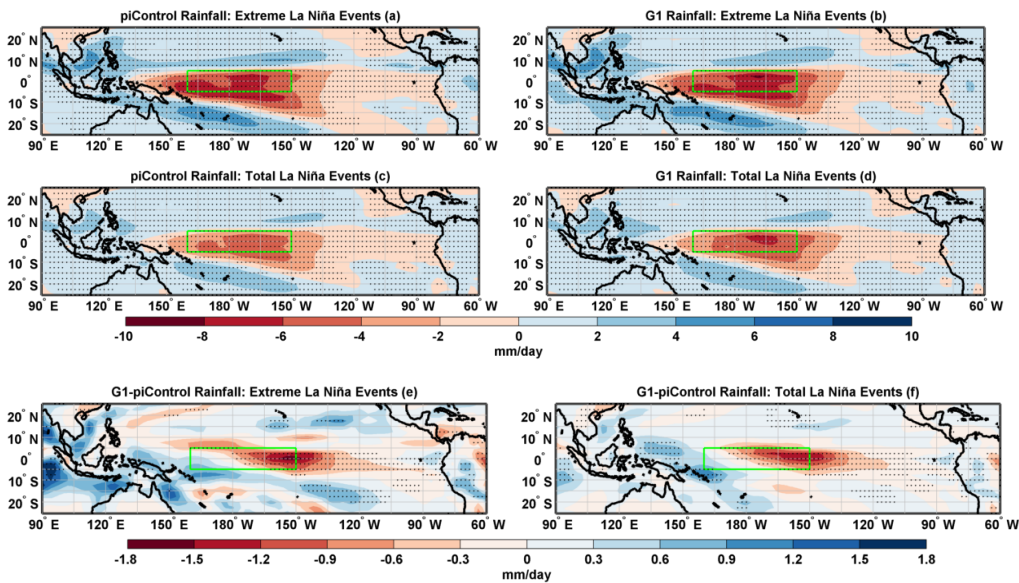
10

11

12

13

14



1

2

3 **Figure 13.** Composites of rainfall anomalies for extreme La Niña events in (a) piControl and
 4 (b) G1. Composites of rainfall anomalies for the total number of La Niña events in (c)
 5 piControl and (d) G1. Composite differences (G1-piControl) of rainfall for (e) extreme La
 6 Niña events and (f) the total number of La Niña events. Stipples indicate grid points with
 7 statistical significance at 99-% cl using a non-parametric Wilcoxon rank-sum test. The green
 8 box indicates the Niño4 region.

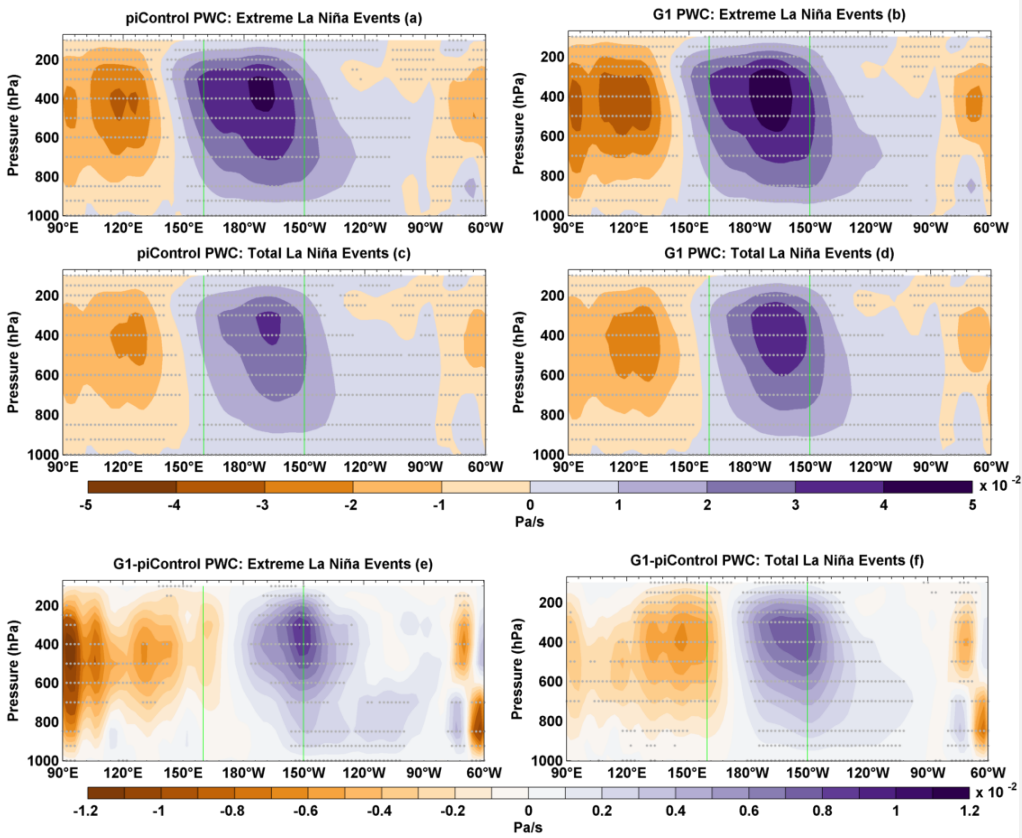
9

10

11

12

13



1

2

3

4

5

6

7

8

9

10

11

12

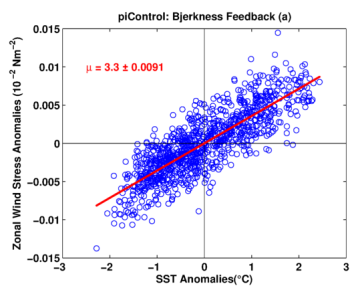
13

14

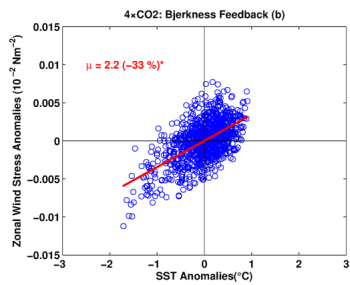
15

16

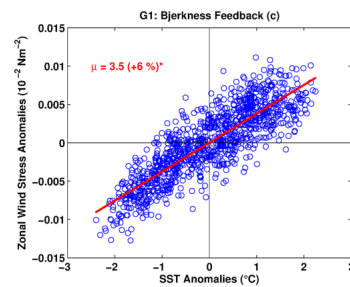
Figure 14. Composites of PWC anomalies for extreme La Niña events in (a) piControl and (b) G1. Composites of PWC for the total number of La Niña events in (c) piControl and (d) G1. Composite differences (G1-piControl) of PWC anomalies for (e) extreme La Niña events and (f) the total number of La Niña events. Stipples indicate grid points with statistical significance at 99-% cl using a non-parametric Wilcoxon rank-sum test. The green vertical lines indicate the Niño4 region.



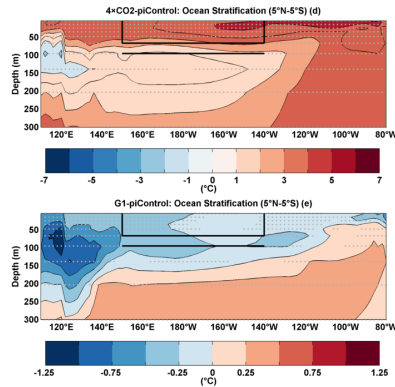
1



2



3



4 **Figure 15.** BJ feedback (μ ; $10^{-2} \text{ Nm}^{-2}/^{\circ}\text{C}$) for (a) piControl (b) $4\times\text{CO}_2$, and (c) G1. The value
 5 with \pm sign indicates s.d. of μ after 10,000 bootstrap ~~realizations~~realisations. An asterisk
 6 indicates statistical significance at 99-% c.l. Mean change in ocean temperature, (d) $4\times\text{CO}_2$ -
 7 piControl, and (e) G1-piControl. The black box shows the area averaging region for upper
 8 ocean temperature, and the black line shows the lower layer used for calculation of
 9 stratification as a difference of upper and lower layer. Stipples indicate grid points with
 10 statistical significance at 99-% c.l. using a non-parametric Wilcoxon rank-sum test.

11

12

13

14

15

16

1

2 **Tables and Table Captions**3 **Table 1.** Eastern Pacific ENSO amplitude

Experiment	Amplitude (°C)	Difference w.r.t. piControl (°C)	Std. Dev. 10,000 Realizations (°C)	~ Change w.r.t. piControl (%)
piControl	1.04 [1.03]		0.0213 [0.03]	
4×CO ₂	0.55 [0.85]	-0.49 [-0.18]		-47* [-17*]
G1	1.13 [1.13]	0.09 [0.1]		+9* [+10**]

4 Key: Niño3 [E-Index]; *99-% cl; **95-% cl

5

6 **Table 2.** Central Pacific ENSO amplitude

Experiment	Amplitude (°C)	Difference w.r.t. piControl (°C)	Std. Dev. 10,000 Realizations (°C)	~ Change w.r.t. piControl (%)
piControl	(0.78) [0.85]		(0.0132) [0.0167]	
4×CO ₂	(0.28) [0.53]	(-0.50) [-0.32]		(-64*) [-38*]
G1	(0.79) [0.83]	(0.01) [0.03]		(+1) [-3]

7 Key: (Niño4) [C-Index]; *99-% cl; **95-% cl

8

9 **Table 3.** Maximum amplitude of warm events

Experiment	Amplitude (°C)	Difference w.r.t. piControl (°C)	Std. Dev. 10,000 Realizations (°C)	~ Change w.r.t. piControl (%)
piControl	2.97 [4.59]		0.0687 [0.2342]	
4×CO ₂	1.29 [3.65]	-1.68 [-0.94]		-57* [-21*]
G1	2.85 [4.33]	-0.12 [-0.26]		-4 [-6]

10 Key: Niño3 [E-Index]; *99-% cl; **95-% cl

11

12 **Table 4.** Maximum amplitude of cold events

Experiment	Amplitude (°C)	Difference w.r.t. piControl (°C)	Std. Dev. 10,000 Realizations (°C)	~ Change w.r.t. piControl (%)
piControl	(-2.13) [-2.47]		(0.0459) [0.1452]	
4×CO ₂	(-1.37) [-2.17]	(-0.76) [-0.30]		(-36*) [-12*]
G1	(-2.55) [-2.90]	(0.42) [0.43]		(+20*) [+17*]

13 Key: (Niño4) [C-Index]; *99-% cl; **95-% cl

14

15 **Table 5.** Niño3 SST skewness

Experiment	Skewness	Difference w.r.t. piControl	Std. Dev. 10,000 Realizations	~ Change w.r.t. piControl (%)
piControl	0.52*		0.0542	
4×CO ₂	-0.47*	-0.99		-190*
G1	0.18*	-0.34		-65*

16 Key: *99-% cl; **95-% cl